

PROPAGATION OF LOCALISED PERTURBATIONS IN GRANULAR MATERIALS

Research Report Mech 287/07

Lauri Ilison, Andrus Salupere

*Centre for Nonlinear Studies, Institute of Cybernetics at Tallinn University of
Technology, Akadeemia tee 21, 12618, Tallinn, Estonia*

Abstract

Wave propagation in dilatant granular materials is studied by making use of a hierarchical Korteweg–de Vries type evolution equation. The model equation is solved numerically under sech^2 -type initial conditions. The behavior of the solution is described and analysed over a wide range of material parameters (two dispersion parameters and one microstructure parameter). Five solution types are defined and discussed. The solitonic character of the solution is discussed for all solution types.

Key words: Dilatant granular materials, Solitons, Wave hierarchies, Korteweg–de Vries type evolution equations

1 Introduction

Many physical and technological applications deal with nonlinear wave propagation in continuous media with microstructure. Granular materials could be an example of such microstructured materials [1–3]. The flow behavior of a granular material is usually considered to be similar to the fluid behavior except that its response depends on the distribution of the volume fraction in the reference placement. The introduction of the volume fraction of the grains

Email addresses: lauri@cens.ioc.ee (Lauri Ilison), salupere@ioc.ee (Andrus Salupere).

as an independent kinematical variable, in order to describe the local deformations of the grains themselves, requires an additional balance equation for the microinertia [3]. In dynamics the most important scale factor is an averaged diameter of a grain that must be related to the wavelength of the excitation (i.e. propagating wave). A physically consistent derivation of the governing mathematical model of dilatant granular materials is given by Giovine and Oliveri [1]. In one-dimensional setting the governing equation is

$$\frac{\partial u}{\partial t} + u \frac{\partial u}{\partial x} + \alpha_1 \frac{\partial^3 u}{\partial x^3} + \beta \frac{\partial^2}{\partial x^2} \left(\frac{\partial u}{\partial t} + u \frac{\partial u}{\partial x} + \alpha_2 \frac{\partial^3 u}{\partial x^3} \right) = 0 \quad (1)$$

where α_1 , α_2 are dispersion parameters and β is a parameter involving the ratio of the grain size and the wavelength. Equation (1) consists of two Korteweg–de Vries (KdV) operators: the first describes the motion in the macrostructure and the second (in the brackets) — the motion in the microstructure. Equation (1) is clearly hierarchical in the Whitham’s sense — if parameter β is small then the influence of the microstructure can be neglected and the wave “feels” only macrostructure [4]. If, however, parameter β is large, then only the influence of the microstructure “is felt” by the wave. Due to that kind of hierarchy the equation (1) could be called as a hierarchical Korteweg–de Vries (HKdV) equation.

In course of time different authors have given different definitions of solitons. Remoissenet [5] brings to light three concepts. The first definition is related to the first documented observation of solitary water wave by John Scott Russell:

- A solitary wave, as discovered by Scott Russell, is a localised wave that propagates along one space direction only, with undeformed shape.

The second definition is quite mathematical and is related to integrable systems, i.e. to idealised conditions:

- A soliton, as discovered numerically by Zabusky and Kruskal, is a large amplitude coherent pulse or very stable solitary wave, the exact solution of a wave equation, whose shape and speed are not altered by a collision with other solitary waves.

For physicists, who study the real world, the keyword soliton has weaker meaning. For them the third definition which highlights the importance of a particular type of energy propagation is presented.

- Solitons are localised finite energy states which are fundamentally nonlinear objects and so cannot be reached by perturbation theory from any linear state.

In the present study the soliton concept given by Drazin [6,7] and Zabusky [8] is used. By Drazin [6,7]:

- The term soliton is associated with any solution of a nonlinear equation or system which (i) represents a wave of permanent form; (ii) is localised, so that it decays or approaches a constant at infinity; (iii) can interact strongly with other solitons and retain its identity.

By Zabusky [8]:

- A Soliton is defined as a localised or solitary entity that propagates at a uniform speed and preserves its structure (or shape) and speed in an interaction with another such solitary entity.

Therefore, solitary wave can be called soliton if it propagates at constant speed and shape and restores its speed and shape after interactions. Interactions of such a type are used to call elastic interactions.

The present paper is dedicated to numerical simulation of propagation of localised initial perturbations. Special attention is paid to the solitonic character of solutions. In Section 2 the problem is stated and in Section 3 the numerical method is described. Solution types are defined in Section 4 and in Sections 5–9 different properties of solutions are discussed in details while conclusions are drawn in Section 10.

2 Statement of the problem

In the present paper propagation of solitary waves in dilatant granular materials is studied making use of the HKdV Eq. (1). For this reason the model Eq. (1) is integrated numerically under localised initial and periodic boundary conditions

$$\begin{aligned} u(x, 0) &= A \operatorname{sech}^2 \frac{x}{\delta}, & \delta &= \sqrt{\frac{12\alpha_1}{A}}, \\ u(x + 16k\pi, t) &= u(x, t), & k &= \pm 1, \pm 2, \pm 3, \dots \end{aligned} \quad (2)$$

where A is the amplitude and δ the width of the initial pulse. It is clear that the latter is the analytical solution of KdV equation that corresponds to the first KdV operator in Eq. (1) [9].

The goals of the present paper are:

- (i) to find numerical solutions for the proposed problem (1), (2) over wide range of material parameters (dispersion parameters α_1 and α_2 and mi-

- crostructure parameter β);
- (ii) to characterise the time–space behaviour of solutions and to define solution types;
- (iii) to characterise solutions in terms of spectral characteristics (spectral densities and time averaged spectral densities);
- (iv) to analyse results over 3 dimensional domain of material parameters α_1 , α_2 and β ;
- (v) to estimate the influence of the amplitude of the initial solitary wave on the character of the solution.

3 Numerical method

For numerical integration of the HKdV equation the pseudospectral method (PsM) [10–13] is applied. In a nutshell, the idea of the PsM is to approximate space derivatives by a certain global method — reducing thereby partial differential equation to ordinary differential equation (ODE) — and to apply a certain ODE solver for integration with respect to the time variable. In the present paper space derivatives are found making use the discrete Fourier transform (DFT),

$$U(k, t) = Fu = \sum_{j=0}^{n-1} u(j\Delta x, t) \exp\left(-\frac{2\pi ijk}{n}\right), \quad (3)$$

where n is the number of space-grid points, $\Delta x = 2\pi/n$ space step, i imaginary unit, $k = 0, \pm 1, \pm 2, \dots, \pm(n/2 - 1), -n/2$ and F denotes the DFT. The usual PsM algorithm (derived for $u_t = \Phi(u, u_x, u_{2x}, \dots, u_{nx})$ type equations) needs to be modified due to the existence of the mixed partial derivative in the HKdV equation (1).

At first the HKdV equation is rewritten in the form

$$(u + \beta u_{2x})_t + (u + 3\beta u_{2x})u_x + (\alpha_1 + \beta u)u_{3x} + \beta\alpha_2 u_{5x} = 0 \quad (4)$$

and a variable

$$v = u + \beta u_{2x} \quad (5)$$

is introduced. Making use the Fourier transform the last expression can be rewritten in the form

$$v = F^{-1} [F(u)] + \beta F^{-1} [-k^2 F(u)] = F^{-1} [(1 - \beta k^2) F(u)] \quad (6)$$

where F^{-1} denotes the inverse Fourier transform. From expression (6) the

variable u can be explicit in the form

$$u = F^{-1} \left[\frac{F(v)}{1 - \beta k^2} \right]. \quad (7)$$

Now the space derivatives of u can be expressed in the terms of v

$$\frac{\partial^n u}{\partial x^n} = F^{-1} \left[\frac{(ik)^n F(v)}{1 - \beta k^2} \right]. \quad (8)$$

Finally, equation (6) can be rewritten in the terms of variable v

$$v_t = -(u + 3\beta u_{2x})u_x - (\alpha_1 + \beta u)u_{3x} - \alpha_2\beta u_{5x}. \quad (9)$$

In equation (9) the variable u and all its space derivatives could be expressed in terms of v accordingly to expressions (5), (7) and (8). Therefore equation (9) can be considered as an ODE with respect to the variable v and could be integrated numerically making use standard ODE solvers.

Calculations are carried out using SciPy package [14]: for DFT the FFTW [15] library and for ODE solver the F2PY [16] generated Python interface to ODEPACK Fortran code [17] is used.

3.1 Stability and accuracy of solutions

The question about the stability and the accuracy of solutions certainly arises with any numerical computation. The studied HKdV equation (1) can be rewritten in the form of first conservation law

$$(u + \beta u_{2x})_t + \left[\frac{u^2}{2} + \alpha_1 u_{2x} + \beta \left(\frac{u^2}{2} + \alpha_2 u_{2x} \right)_{2x} \right]_x = 0 \quad (10)$$

with conserved density

$$C_1(t) = \int_0^{2\pi} (u + \beta u_{2x}) dx \quad (11)$$

and in the form on second conservation law

$$\left\{ \frac{1}{2} \alpha_1 u^2 + \beta \left[(u_x)^2 + uu_{2x} \right] \right\}_t + \left\{ \frac{1}{3} \alpha_1 u^3 + uu_{2x} - \frac{1}{2} (u_x)^2 + \beta \left[\frac{1}{3} \alpha_1 u^3 + uu_{2x} - \frac{1}{2} (u_x)^2 \right]_{2x} \right\}_x = 0 \quad (12)$$

with conserved density

$$C_2(t) = \int_0^{2\pi} \left(\frac{1}{2} \alpha_1 u^2 + \beta [(u_x)^2 + uu_{2x}] \right) dx. \quad (13)$$

In order to estimate the accuracy of computations numerical experiments were carried out with number of space-grid points $n = 512, 1024, 2048, 4096$. The behavior of the conserved density was traced and final wave-profiles $u(x, t_f)$, i.e. the wave-profiles at the end of the integration interval $t = t_f$, were compared. It was found that final wave-profiles for $n \geq 1024$ practically coincide and therefore in numerical experiments below the number of space-grid points $n = 1024$ is used.

In all cases, discussed below, the relative error of the conserved density $C_1(t)$ is less than 10^{-7} . The relative error for $C_2(t)$ is less than 10^{-7} in most cases, however for some sets of parameters when relatively sharp wave profiles emerge with relative error C_2 can have values of order 10^{-2} .

4 Solution types

The HKdV equation (1) is integrated numerically under initial- and boundary conditions (2) for $0 < \alpha_1 < 1$, $0 < \alpha_2 < 1$ and $\beta = 111.11, 11.111, 1.111, 0.111, 0.0111$. The number of space grid points $n = 1024$ and the length of the time interval $t_f = 100$. Based on the analysis of numerical experiments one can introduce five solution types:

- (1) Single KdV soliton
- (2) KdV soliton ensemble
- (3) KdV soliton ensemble with weak tail
- (4) Soliton with strong tail
- (5) Solitary wave with tail and wave packet

At first, in Subsections 4.1–4.5 all solution types are introduced and described in terms of time–slice and pseudocolor plots. In order to comprehend time–slice and pseudocolor plots adequately, one has to remember that: (i) periodic boundary conditions are applied for numerical integration and (ii) all wave profiles are plotted over two space periods. Different properties of solutions, their dependencies on material parameters and on the amplitude of the initial pulse are described and discussed in details in Sections 5–10.

4.1 *The first solution type: Single KdV soliton*

The first solution type is a single KdV soliton, i.e., just a single KdV soliton emerges over time. This solution appears in all cases, where both dispersion parameters α_1 and α_2 have equal values. The different values for initial amplitude A or microstructure parameter β do not change this behavior. As the equation (1) consist of two KdV equations that are tight through the second derivative and as the initial condition is the analytical solution of KdV equation then the result is quite predictable. In Figs. 1–4 two different cases for equal parameters α_1 and α_2 are presented.

The solution could be defined to be soliton as the initial condition is the analytical solution of the KdV equation.

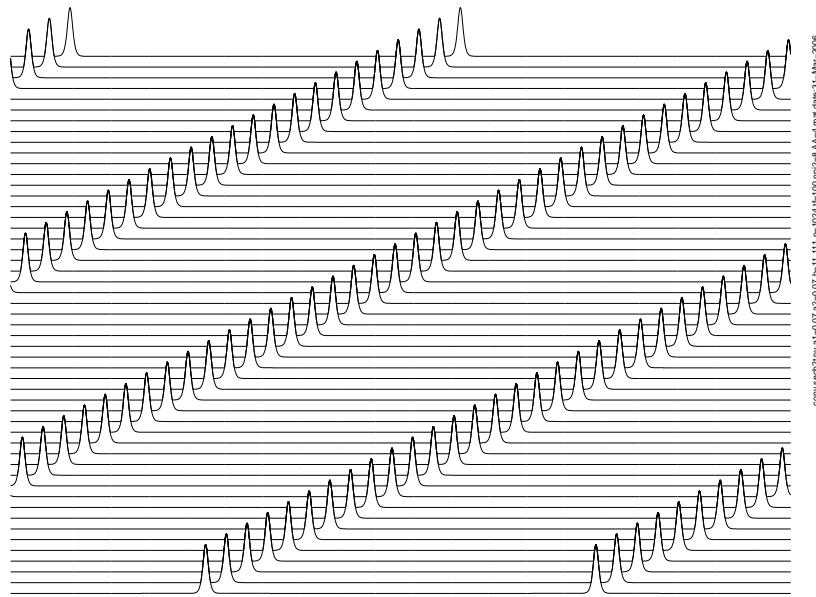


Fig. 1. Single KdV soliton. Time-slice plot over two space periods for $\alpha_1 = 0.07$, $\alpha_2 = 0.07$, $\beta = 11.111$, $n = 1024$, $t_f = 100$, $A = 4$.

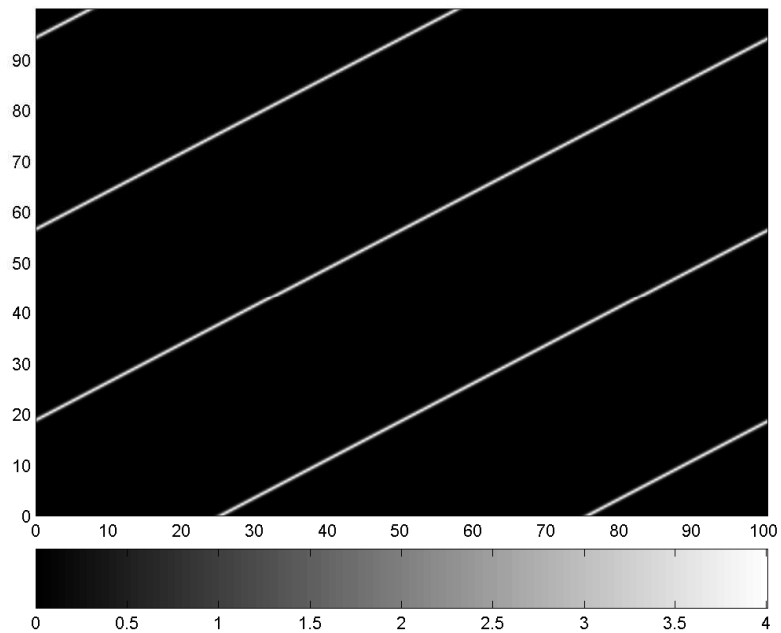


Fig. 2. Single KdV soliton. Pseudocolor plot over two space periods for $\alpha_1 = 0.07$, $\alpha_2 = 0.07$, $\beta = 11.111$, $n = 1024$, $t_f = 100$, $A = 4$.

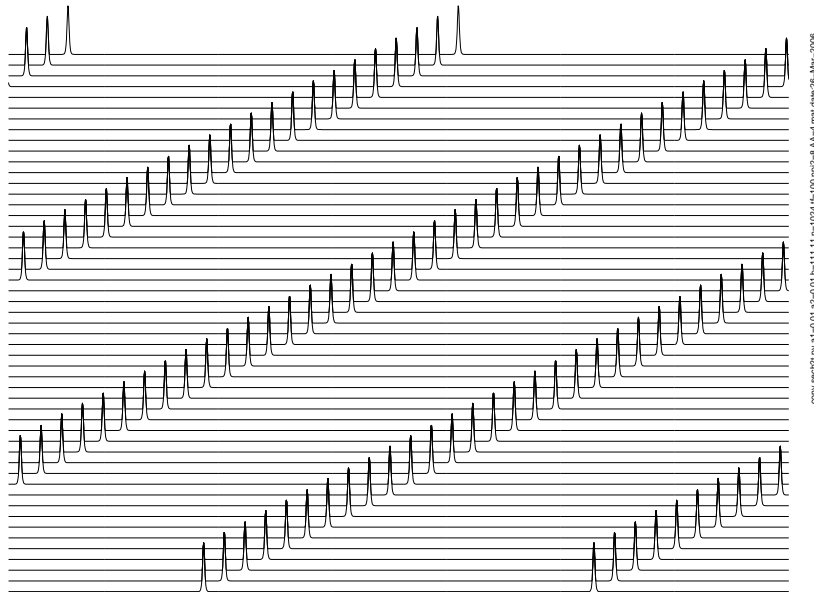


Fig. 3. Single KdV soliton. Time-slice plot over two space periods for $\alpha_1 = 0.01$, $\alpha_2 = 0.01$, $\beta = 111.11$, $n = 1024$, $t_f = 100$, $A = 4$.

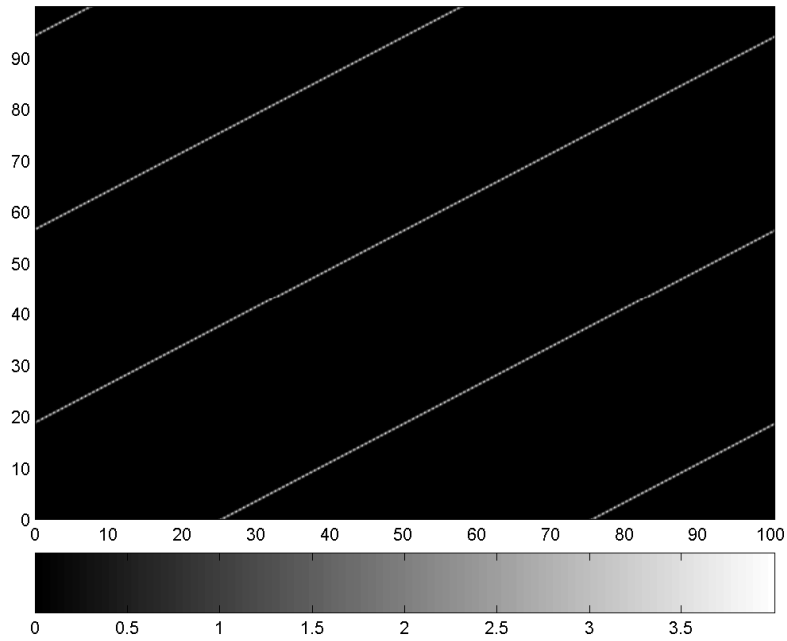


Fig. 4. Single KdV soliton. Pseudocolor plot over two space periods for $\alpha_1 = 0.01$, $\alpha_2 = 0.01$, $\beta = 111.11$, $n = 1024$, $t_f = 100$, $A = 4$.

4.2 The second solution type: KdV soliton ensemble

In case of the second solution type a train of KdV solitons emerge. The number of generated solitons depends on the values of macrostructure dispersion parameter α_1 and microstructure dispersion parameter α_2 . If α_2 is fixed and α_1 increases, then the number of solitons in the KdV ensemble increases. If α_1 is fixed and α_2 increases then the number of solitons decreases up to the limit value 1 (see Sections 5 and 7 for details). In Figs. 5–8 two different cases for this solution type are presented. In Figs. 5–6 ($\alpha_1 = 0.03$ and $\alpha_2 = 0.01$) one has two interacting solitons, but in Figs. 7–8 ($\alpha_1 = 0.4$ and $\alpha_2 = 0.01$) the number of solitons is eight. The number of solitons in the soliton ensemble decreases if α_1 is fixed and α_2 increases or increases if α_2 is fixed and α_1 increases.

The solution type is soliton ensemble as the KdV solitons restore their shape and speed after the interaction.

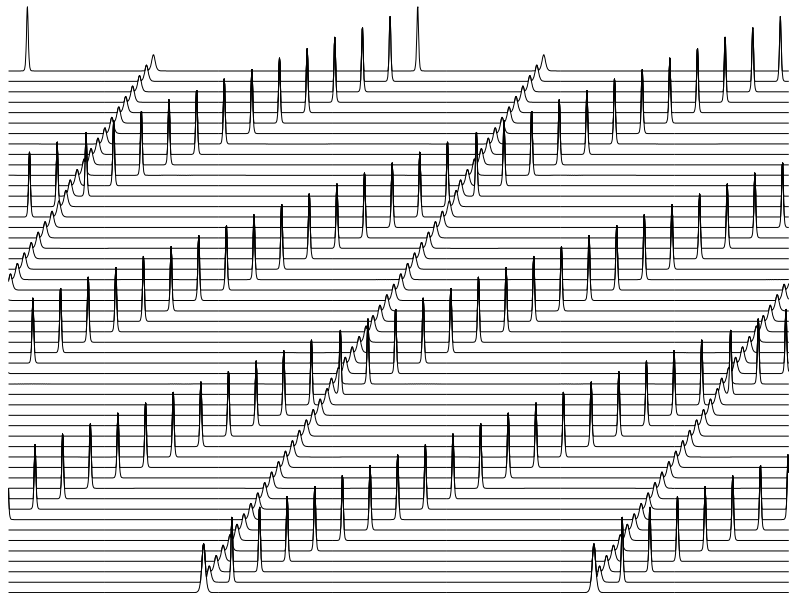


Fig. 5. KdV soliton ensemble. Time-slice plot over two space periods for $\alpha_1 = 0.03$, $\alpha_2 = 0.01$, $\beta = 11.111$, $n = 1024$, $t_f = 100$, $A = 4$.

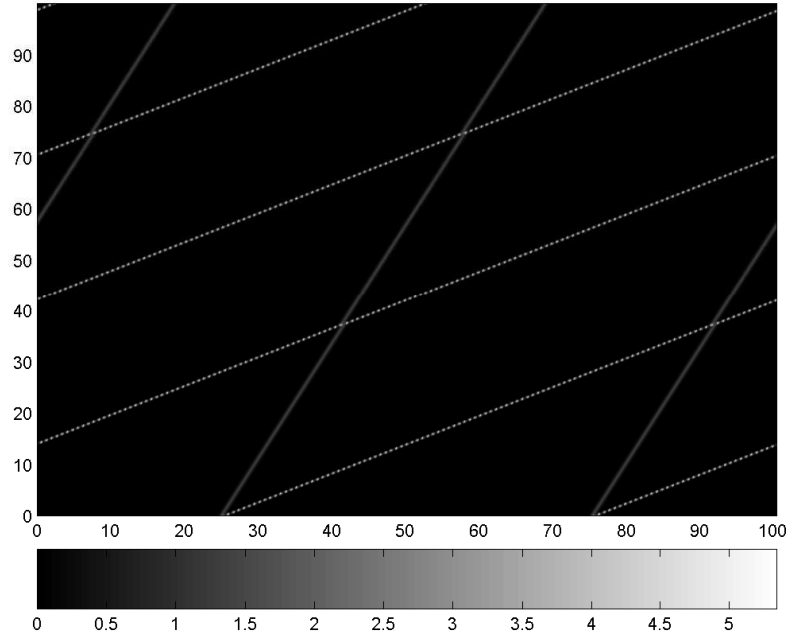


Fig. 6. KdV soliton ensemble. Pseudocolor plot over two space periods for $\alpha_1 = 0.03$, $\alpha_2 = 0.01$, $\beta = 11.111$, $n = 1024$, $t_f = 100$, $A = 4$.

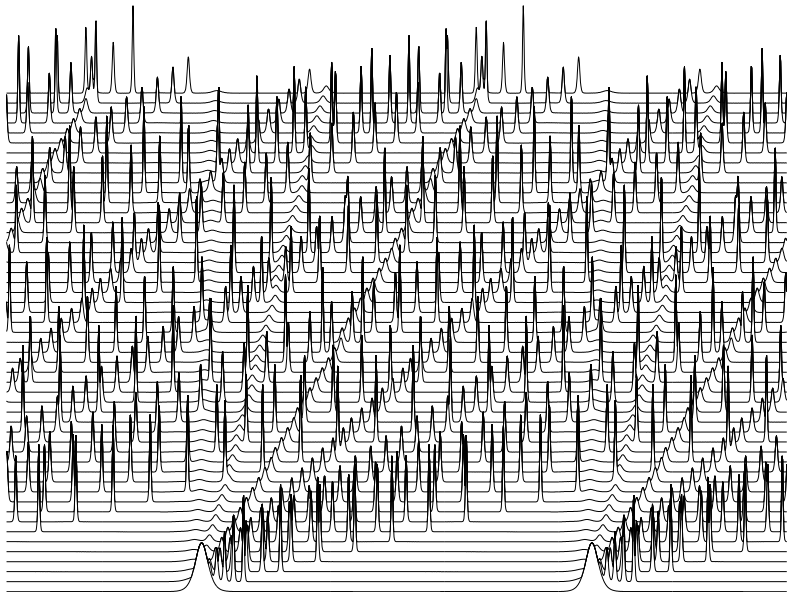


Fig. 7. KdV soliton ensemble. Time-slice plot over two space periods for $\alpha_1 = 0.4$, $\alpha_2 = 0.01$, $\beta = 111.11$, $n = 1024$, $t_f = 100$, $A = 4$.

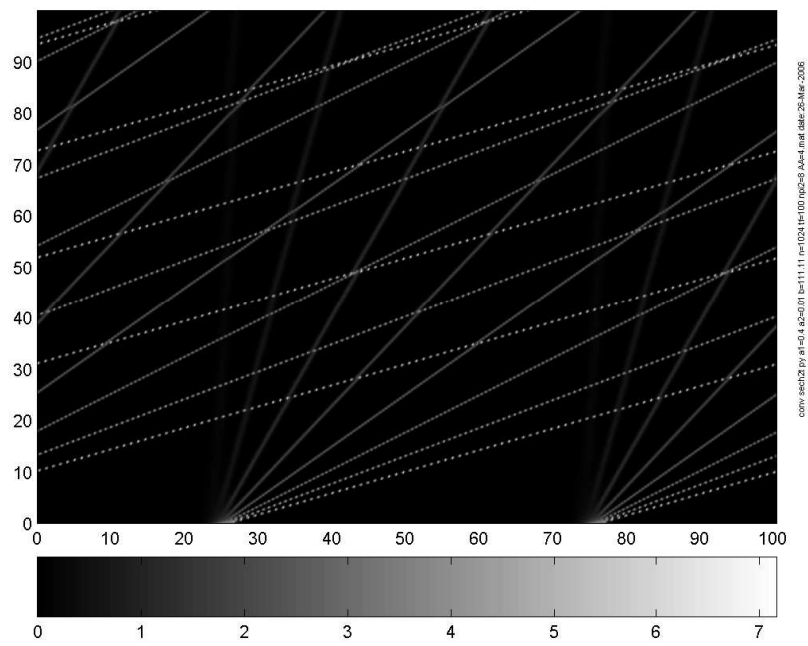


Fig. 8. KdV soliton ensemble. Pseudocolor plot over two space periods for $\alpha_1 = 0.4$, $\alpha_2 = 0.01$, $\beta = 111.11$, $n = 1024$, $t_f = 100$, $A = 4$.

4.3 The third solution type: KdV soliton ensemble with weak tail

In case of the third solution type a train of KdV solitons and a weak tail emerge. The number of KdV solitons in the ensemble depends on dispersion parameters α_1 and α_2 by the same rule as in the case of the second type — if α_2 is fixed and α_1 increases, then the number of solitons in the KdV ensemble increases and vice versa. The weakness of the tail is expressed through the fact that the tail does not influence the behaviour of the KdV ensemble essentially, i.e. here the behaviour of the KdV ensemble is similar to that of the second solution type. In Figs. 9–14 two different cases for this solution type are presented.

The solution type is soliton ensemble as the solitons in the train interact with each other and restore their shape and speed after the interactions. In this case the amplitude of the higher (in case when one has two solitons in the train) or highest (in case when the number of solitons in the train is higher than two) KdV soliton always increases compared to the initial amplitude A . Such a behaviour is typical for the KdV equation — if a train of solitons (and a tail) emerge from initial localised pulse, then the amplitude of the highest soliton in the train is always higher than the amplitude of the initial pulse [7].

Formation of the solution and elastic interactions between solitons can be traced in Figs. 9 and 11 for $\alpha_1 = 0.07$, $\alpha_2 = 0.03$, $\beta = 11.111$ and in Figs. 12 and 14 for $\alpha_1 = 0.4$, $\alpha_2 = 0.1$, $\beta = 111.11$. The shape and the size of tail is clearly visible in Figs. 10 and 13.

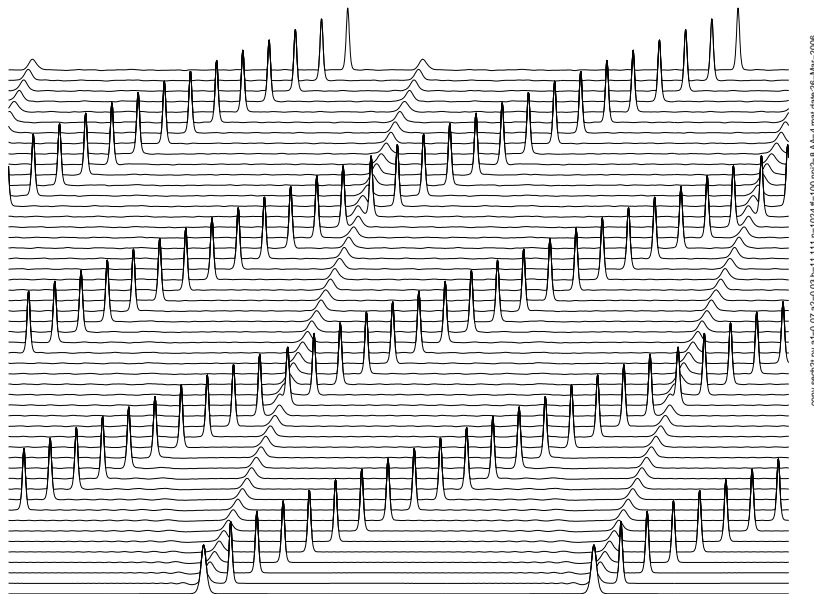


Fig. 9. KdV soliton ensemble with weak tail. Time-slice plot over two space periods for $\alpha_1 = 0.07$, $\alpha_2 = 0.03$, $\beta = 11.111$, $n = 1024$, $t_f = 100$, $A = 4$.

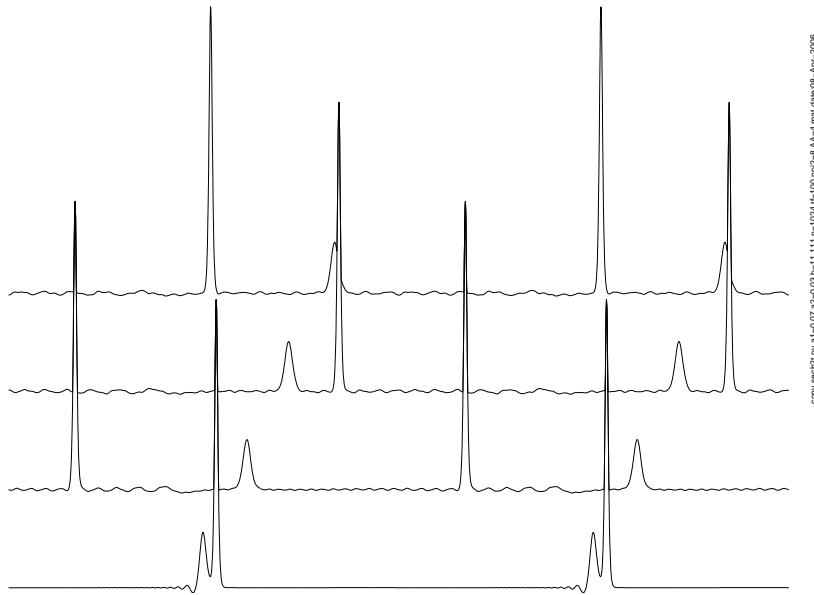


Fig. 10. KdV soliton ensemble with weak tail. Single wave-profiles at $t = 1$, $t = 20$, $t = 40$, $t = 60$ over two space periods for $\alpha_1 = 0.07$, $\alpha_2 = 0.03$, $\beta = 11.111$, $n = 1024$, $t_f = 100$, $A = 4$.

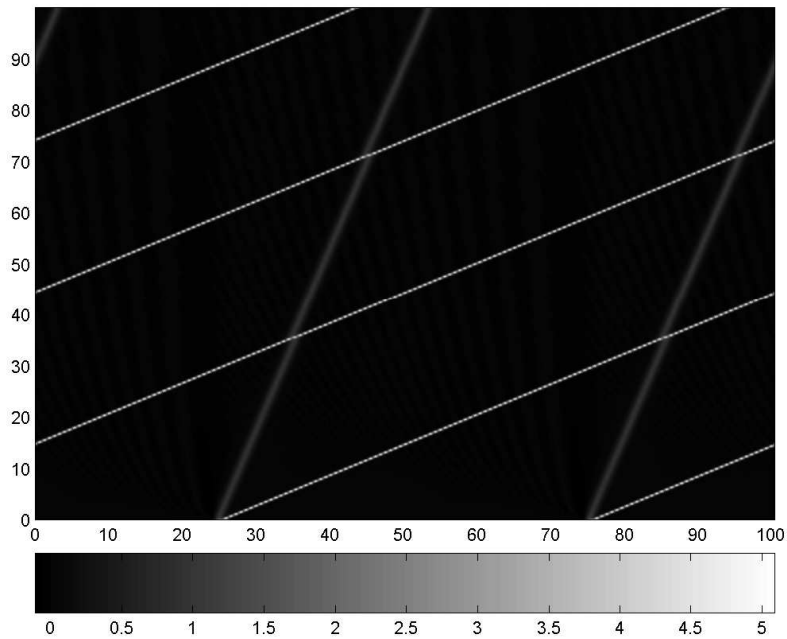


Fig. 11. KdV soliton ensemble with weak tail. Pseudocolor plot over two space periods for $\alpha_1 = 0.07$, $\alpha_2 = 0.03$, $\beta = 11.111$, $n = 1024$, $t_f = 100$, $A = 4$.

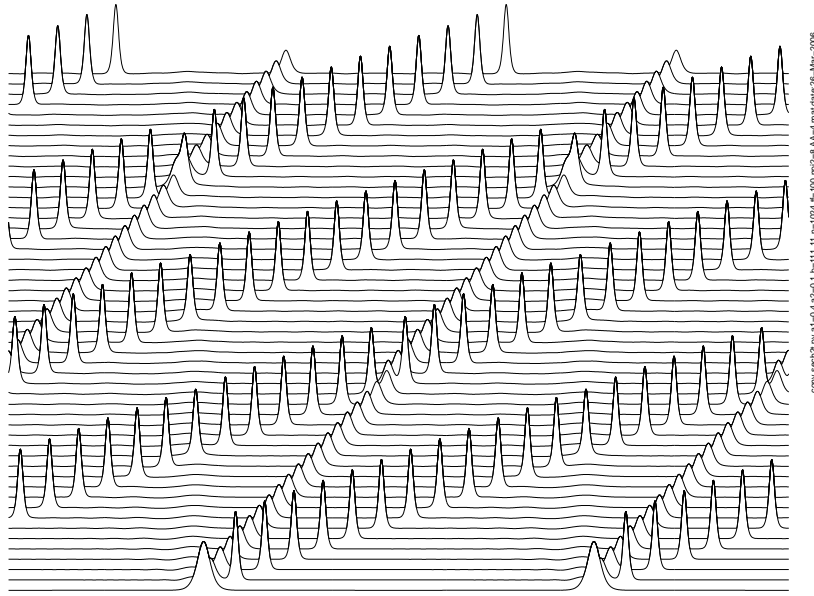


Fig. 12. KdV soliton ensemble with weak tail. Time-slice plot over two space periods for $\alpha_1 = 0.4$, $\alpha_2 = 0.1$, $\beta = 111.11$, $n = 1024$, $t_f = 100$, $A = 4$.

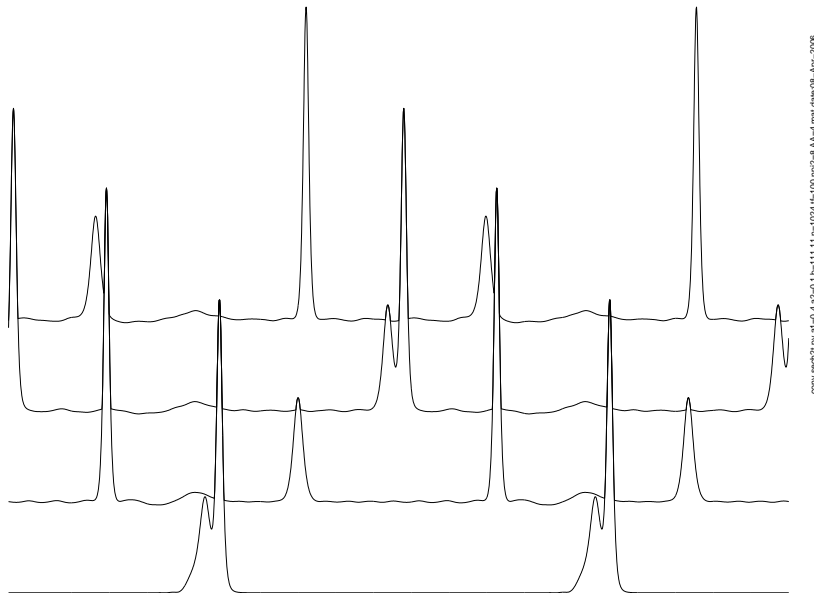


Fig. 13. KdV soliton ensemble with weak tail. Single wave-profiles at $t = 1$, $t = 20$, $t = 40$, $t = 60$ over two space periods for $\alpha_1 = 0.4$, $\alpha_2 = 0.1$, $\beta = 111.11$, $n = 1024$, $t_f = 100$, $A = 4$.

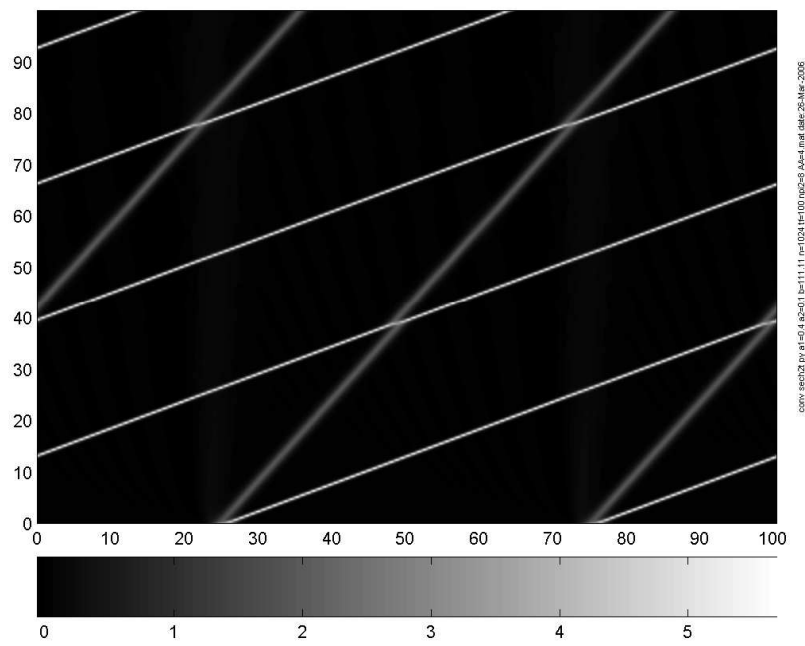


Fig. 14. KdV soliton ensemble with weak tail. Pseudocolor plot over two space periods for $\alpha_1 = 0.4$, $\alpha_2 = 0.1$, $\beta = 111.11$, $n = 1024$, $t_f = 100$, $A = 4$.

4.4 The fourth solution type: Soliton with strong tail

In case of the fourth solution type single soliton and a strong tail emerge. The number of generated oscillations in the tail depends on values of macrostructure dispersion parameter α_1 and microstructure dispersion parameter α_2 .

The behaviour of the solution is strongly influenced by the tail — the amplitude of the soliton is lower than the initial amplitude and the other KdV solitons are suppressed. Such a phenomenon is called selection in [18].

In Figs. 15–20 two different cases for this solution type are presented. In Figs. 15, 17, 18 and 20 formation of the solution and interaction between the KdV soliton and the tail is presented. The size and the shape of the tail can be estimated in Figs. 16 and 19.

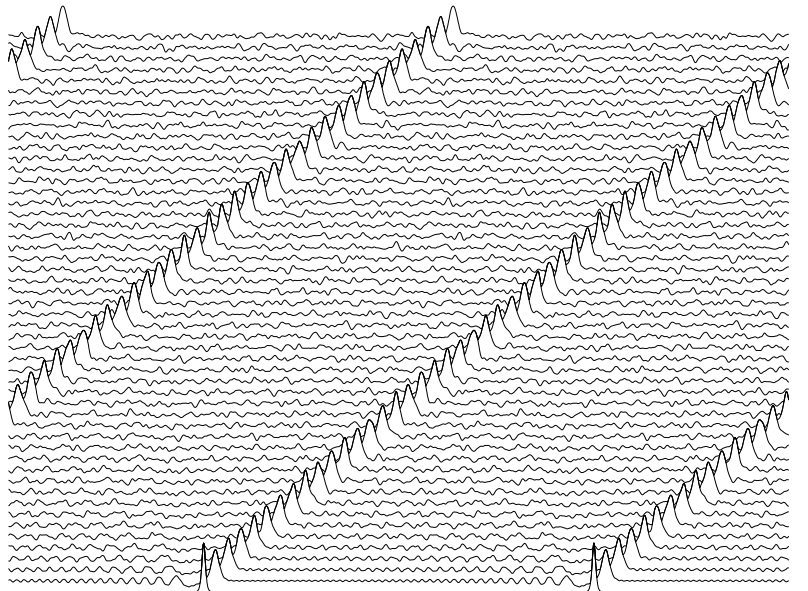


Fig. 15. Soliton with strong tail. Time-slice plot over two space periods for $\alpha_1 = 0.03$, $\alpha_2 = 0.09$, $\beta = 11.111$, $n = 1024$, $t_f = 100$, $A = 4$.

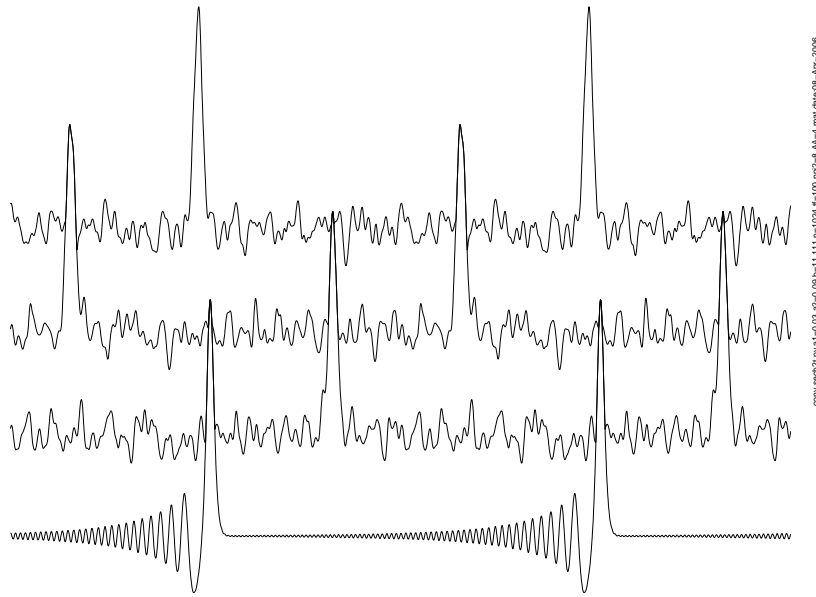


Fig. 16. Soliton with strong tail. Single wave-profiles at $t = 1, t = 20, t = 40, t = 60$ over two space periods for $\alpha_1 = 0.03, \alpha_2 = 0.09, \beta = 11.111, n = 1024, A = 4$.

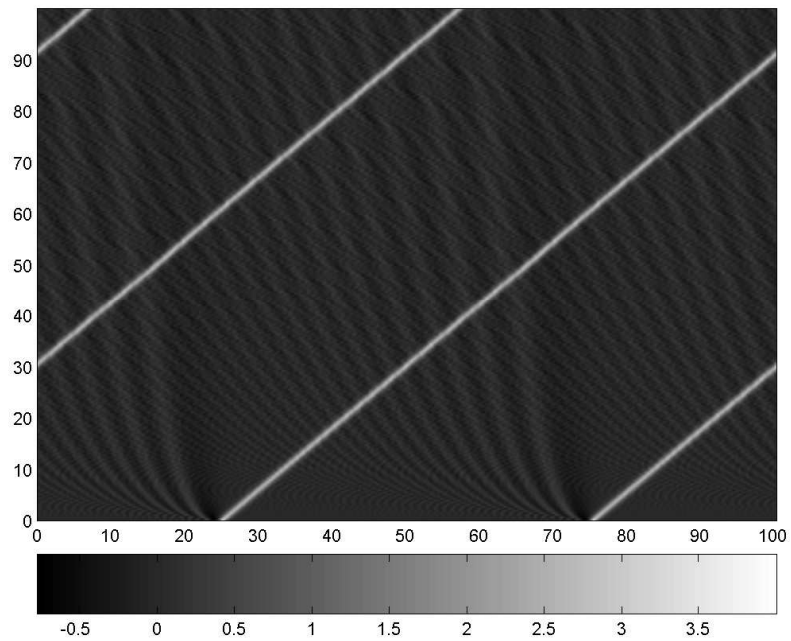


Fig. 17. Soliton with strong tail. Pseudocolor plot over two space periods for $\alpha_1 = 0.03, \alpha_2 = 0.09, \beta = 11.111, n = 1024, t_f = 100, A = 4$.

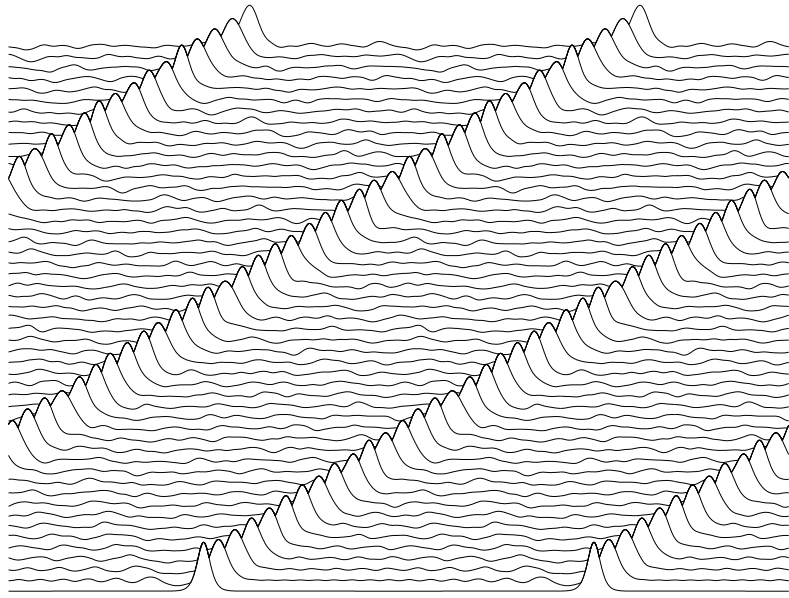


Fig. 18. Soliton with strong tail. Time-slice plot over two space periods for $\alpha_1 = 0.4$, $\alpha_2 = 0.7$, $\beta = 111.11$, $n = 1024$, $t_f = 100$, $A = 4$.

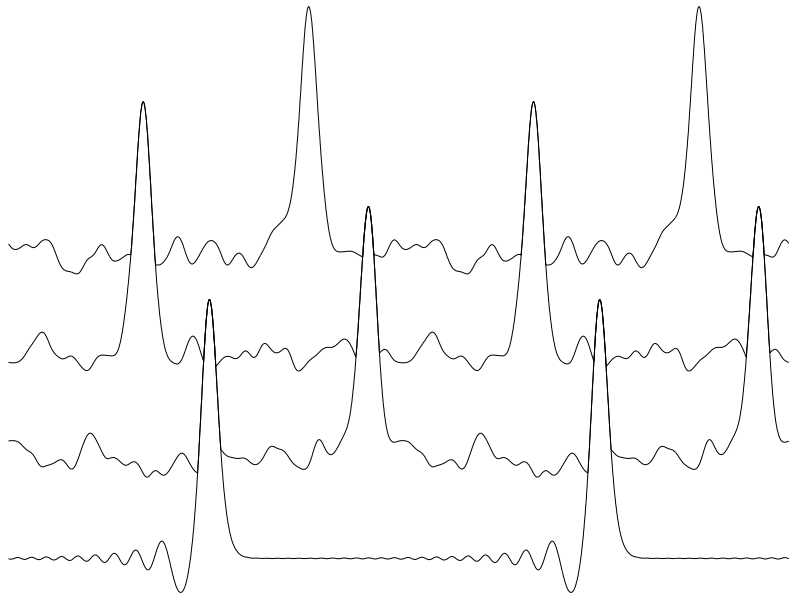


Fig. 19. Soliton with strong tail. Single wave-profiles at $t = 1$, $t = 20$, $t = 40$, $t = 60$ over two space periods for $\alpha_1 = 0.4$, $\alpha_2 = 0.7$, $\beta = 111.11$, $n = 1024$, $A = 4$.

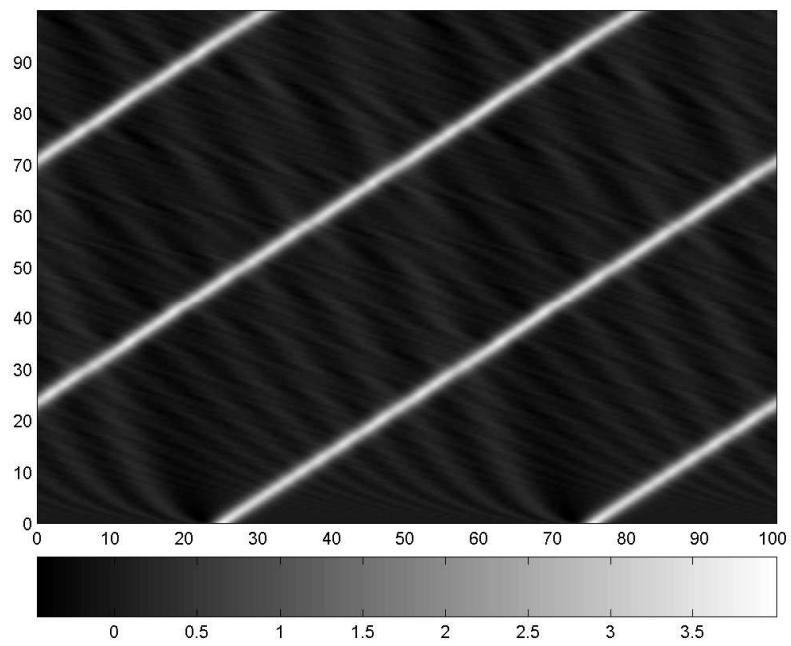


Fig. 20. Soliton with strong tail. Pseudocolor plot over two space periods for $\alpha_1 = 0.4$, $\alpha_2 = 0.7$, $\beta = 111.11$, $n = 1024$, $t_f = 100$, $A = 4$.

4.5 The fifth solution type: Solitary wave with tail and wave packet

In case of the fifth solution type one solitary wave, a tail and wave packet(s) emerge simultaneously. Similar situation is described by Christov and Velarde in [19]. The wave packet is formed by several higher harmonics that are amplified (see Section 9 for details). This phenomenon could be described similarly to sum of two or more harmonic waves having nearly equal frequencies. The envelope of the packet can propagate to the left or to the right and at much higher speed than that of the solitary wave or high frequency waves that form the packet. The solution is stable, i.e., all three components of the solution are conserved over long time intervals. As a rule three different interactions take place in the present case: (i) solitary wave — tail; (ii) solitary wave — wave packet; (iii) tail — wave packet. Furthermore, in some cases two or more wave packets that propagate at different speeds emerge and therefore interactions between wave packets can take place. Like in the case of the fourth solution type a selection phenomenon [18] takes place and the amplitude of the propagating solitary wave is lower than the amplitude of the initial wave.

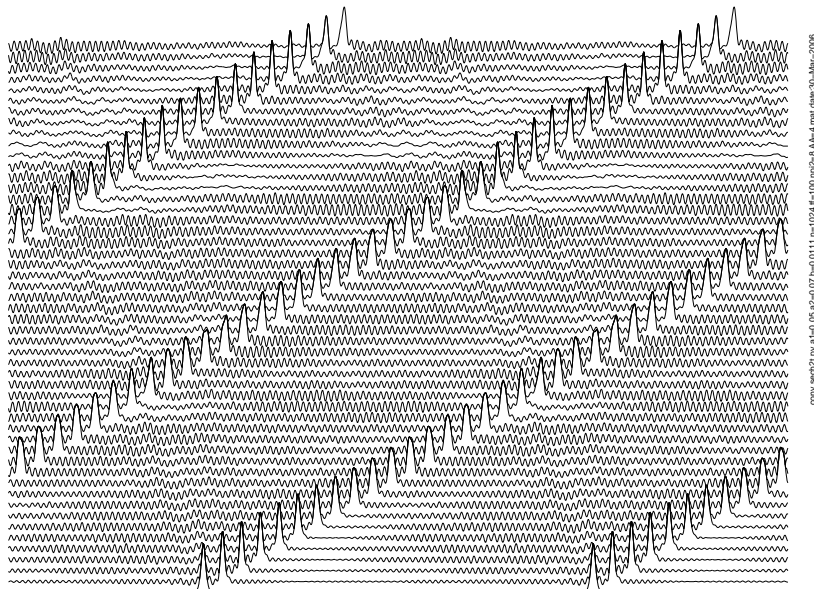


Fig. 21. Solitary wave with tail and wave packet. Time-slice plot over two space periods for $\alpha_1 = 0.05$, $\alpha_2 = 0.07$, $\beta = 0.0111$, $n = 1024$, $t_f = 100$, $A = 4$.

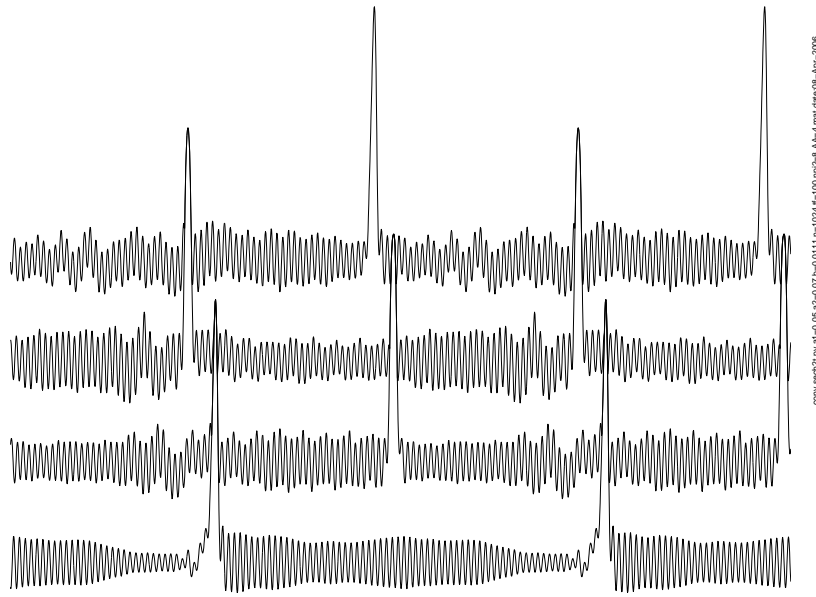


Fig. 22. Solitary wave with tail and wave packet. Single wave-profiles at $t = 1$, $t = 20$, $t = 40$, $t = 60$ over two space periods for $\alpha_1 = 0.05$, $\alpha_2 = 0.07$, $\beta = 0.0111$, $n = 1024$, $A = 4$.

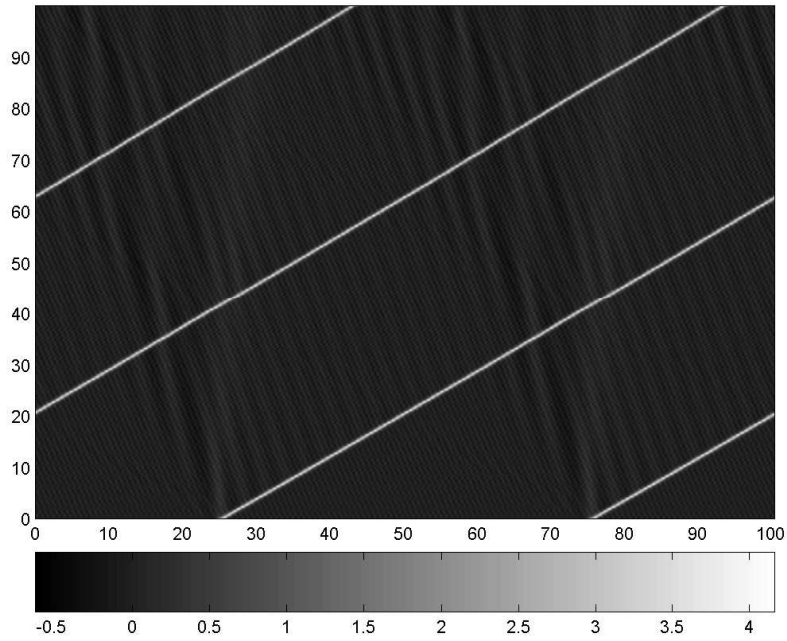


Fig. 23. Solitary wave with tail and wave packet. Pseudocolor plot over two space periods for $\alpha_1 = 0.05$, $\alpha_2 = 0.07$, $\beta = 0.0111$, $n = 1024$, $t_f = 100$, $A = 4$.

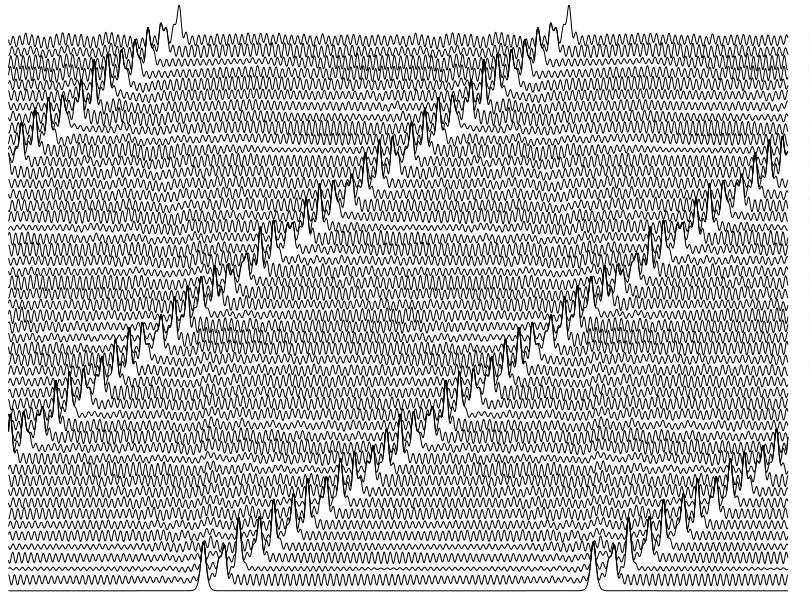


Fig. 24. Solitary wave with tail and wave packet. Time-slice plot over two space periods for $\alpha_1 = 0.07$, $\alpha_2 = 0.11$, $\beta = 0.0111$, $n = 1024$, $t_f = 100$, $A = 4$.

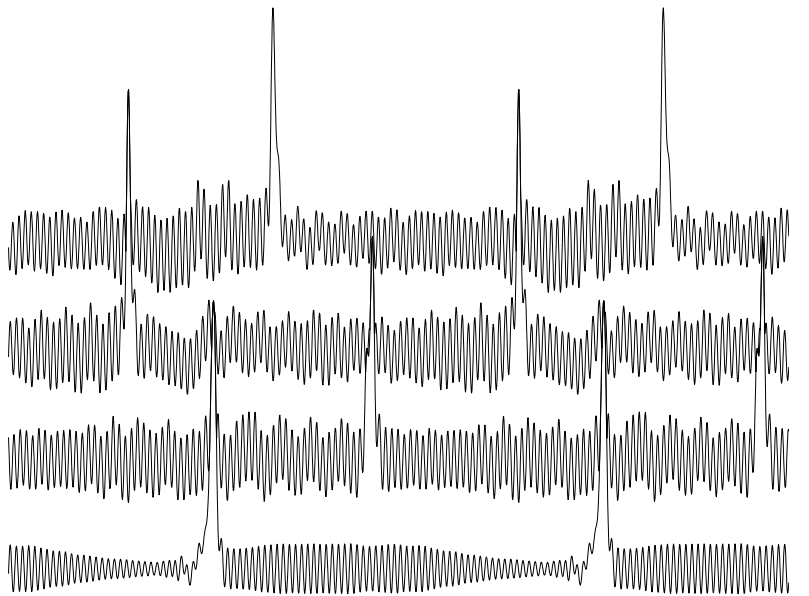


Fig. 25. Solitary wave with tail and wave packet. Single wave-profiles at $t = 1$, $t = 20$, $t = 40$, $t = 60$ over two space periods for $\alpha_1 = 0.07$, $\alpha_2 = 0.11$, $\beta = 0.0111$, $n = 1024$, $A = 4$.

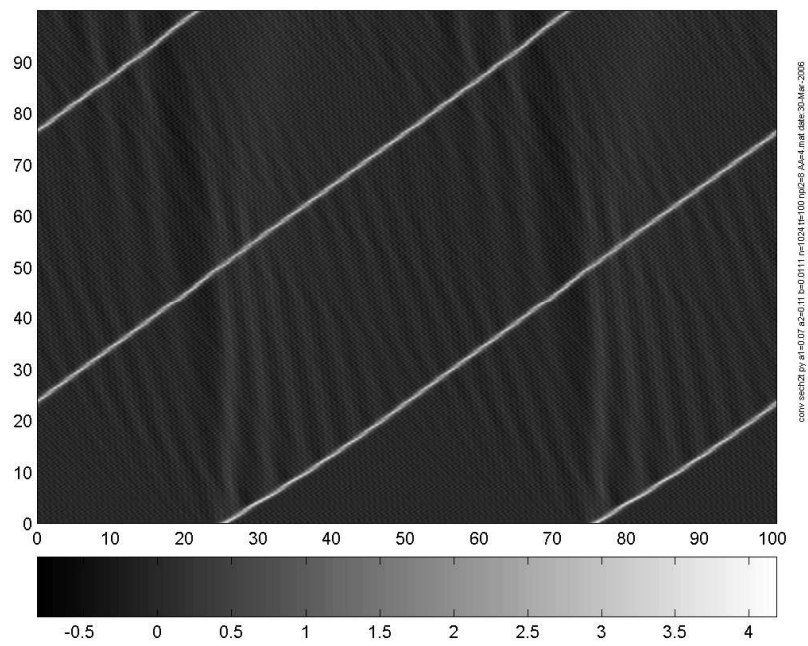


Fig. 26. Solitary wave with tail and wave packet. Pseudocolor plot over two space periods for $\alpha_1 = 0.07$, $\alpha_2 = 0.11$, $\beta = 0.0111$, $n = 1024$, $t_f = 100$, $A = 4$.

4.6 Limit cases

There are some limit cases: (i) Fig. 27 demonstrates the case where the number of KdV solitons is very high and probably the second KdV ensemble forms. (ii) Fig. 28 demonstrates the case where the solitary wave disappears.

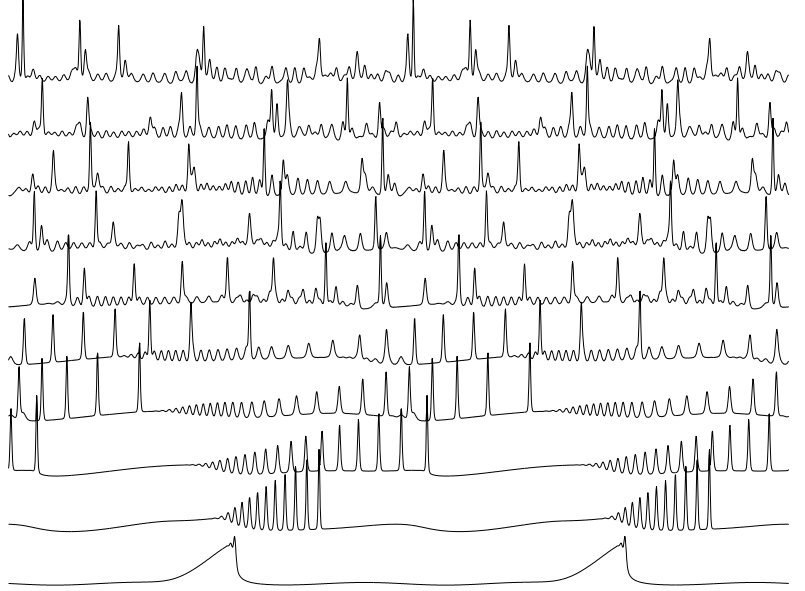


Fig. 27. KdV soliton ensemble. Single wave-profiles at $t = 1, t = 5, t = 10, t = 15, t = 20, t = 30, t = 40, t = 50, t = 60, t = 70$ over two space periods for $\alpha_1 = 2.2, \alpha_2 = 0.01, \beta = 11.111, n = 1024, t_f = 500, A = 4$.

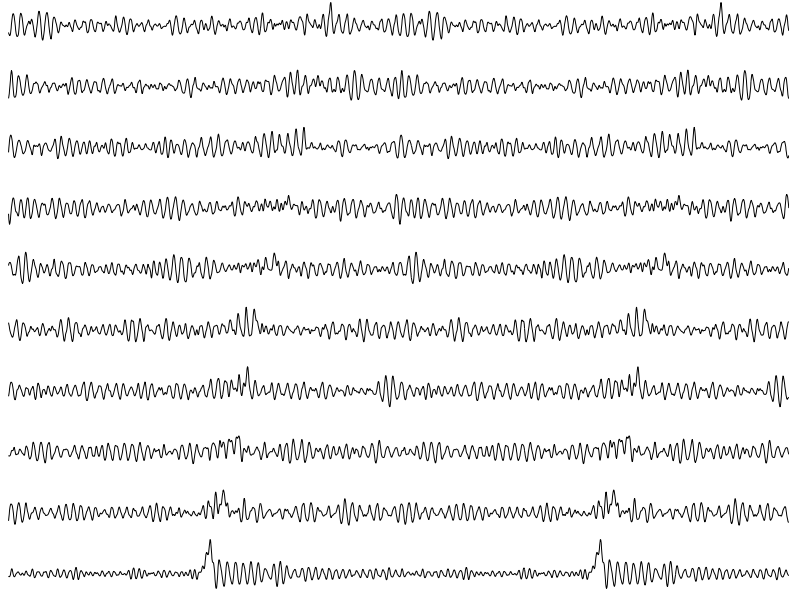


Fig. 28. Solitary wave with tail and packet. Single wave-profiles at $t = 1, t = 5, t = 10, t = 15, t = 20, t = 30, t = 40, t = 50, t = 60, t = 70$ over two space periods for $\alpha_1 = 0.01, \alpha_2 = 0.05, \beta = 0.0111, n = 1024, t_f = 100, A = 4$.

5 Solution types in the dispersion parameter plane

In Figs. 29–33 solution types are presented against the dispersion parameters α_1 and α_2 . Figures are given for different values of microstructure parameter β .

The first solution type appears in case of $\alpha_1 = \alpha_2$ for all values of the microstructure parameter β . The second and the third solution type appears for $\alpha_1 > \alpha_2$ in case of $\beta = 111.11$ and $\beta = 11.111$ (Figs. 29 and 30). The fourth solution type appears for $\alpha_1 < \alpha_2$ in case of $\beta = 111.11$ and $\beta = 11.111$ (Figs. 29 and 30) and for $\alpha_1 > \alpha_2$ in case of $\beta = 0.0111$ (Fig. 33). The fifth solution type can be realised for $\alpha_1 > \alpha_2$ and for $\alpha_1 < \alpha_2$ in case of $\beta = 1.111$ and $\beta = 0.111$ (Figs. 31 and 32) and for $\alpha_1 < \alpha_2$ in case of $\beta = 0.0111$ (Fig. 33).

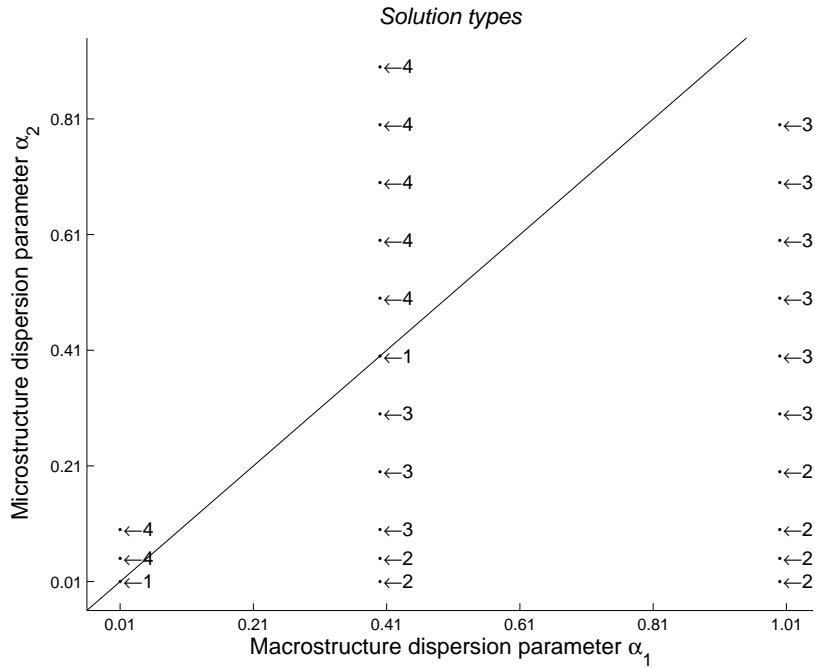


Fig. 29. Solution types in case of $\beta = 111.11$, labels: 1-Single KdV soliton, 2-KdV soliton ensemble, 3-KdV soliton ensemble with weak tail, 4-soliton with strong tail, 5-solitary wave with tail and wave packet.

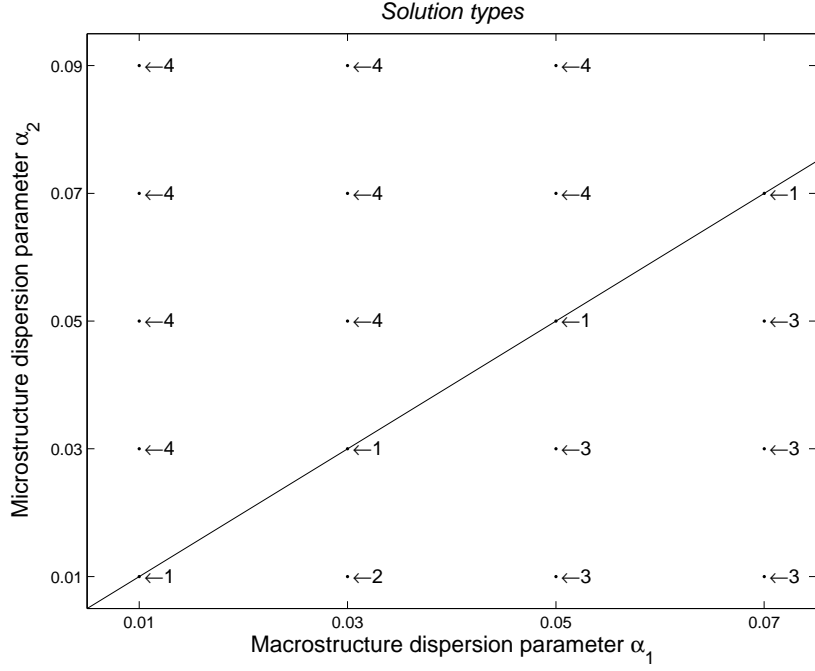


Fig. 30. Solution types in case of $\beta = 11.111$, $n = 1024$, $t_f = 100$, $A = 4$, labels: 1-Single KdV soliton, 2-KdV soliton ensemble, 3-KdV soliton ensemble with weak tail, 4-soliton with strong tail, 5-solitary wave with tail and wave packet.

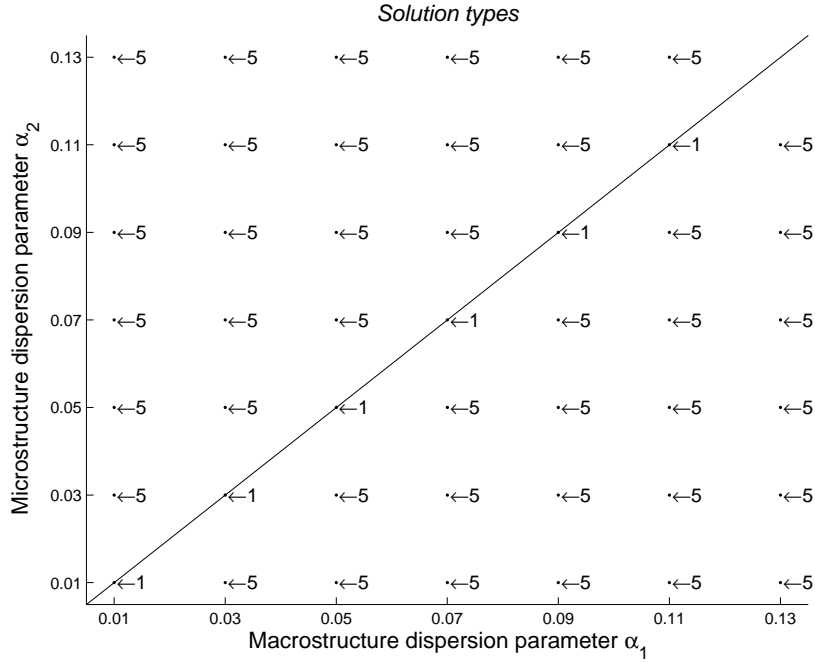


Fig. 31. Solution types in case of $\beta = 1.111$, $n = 1024$, $t_f = 100$, $A = 4$, labels: 1-Single KdV soliton, 2-KdV soliton ensemble, 3-KdV soliton ensemble with weak tail, 4-soliton with strong tail, 5-solitary wave with tail and wave packet.

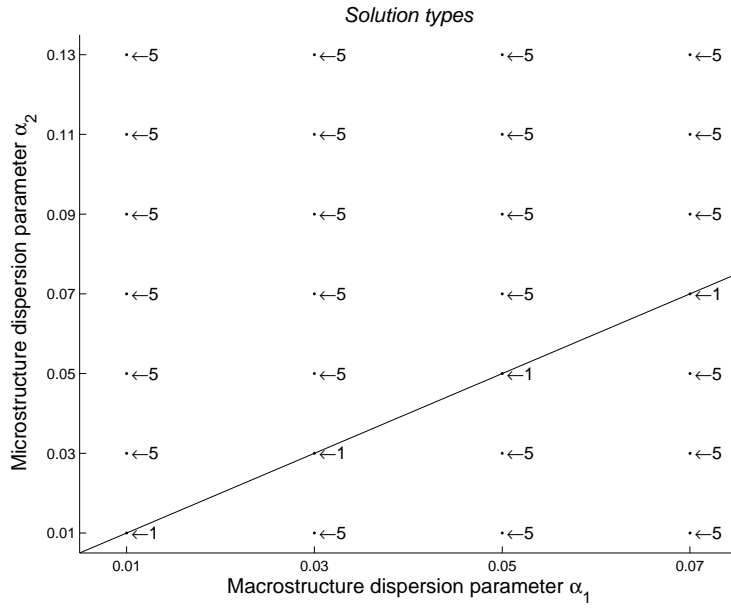


Fig. 32. Solution types in case of $\beta = 0.1111$, $n = 1024$, $t_f = 100$, $A = 4$, labels: 1-Single KdV soliton, 2-KdV soliton ensemble, 3-KdV soliton ensemble with weak tail, 4-soliton with strong tail, 5-solitary wave with tail and wave packet.

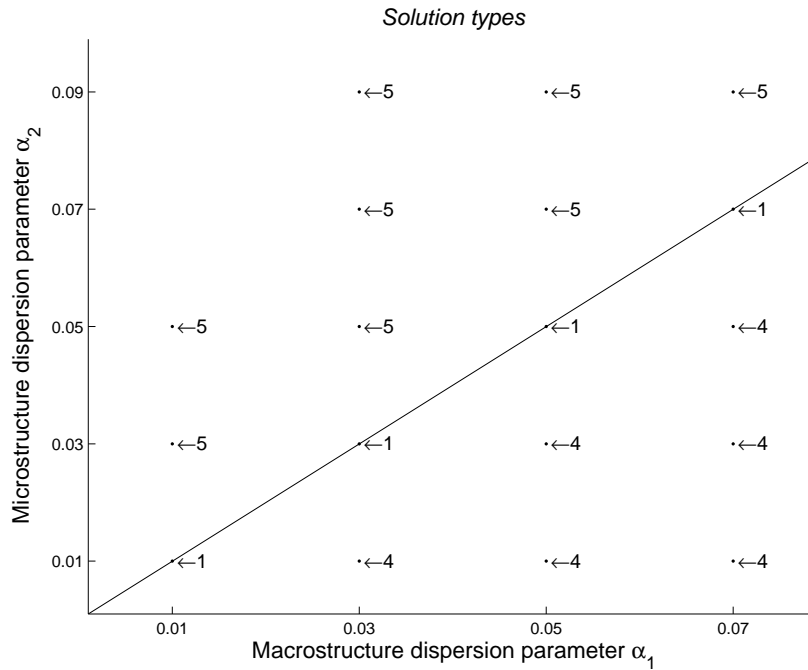


Fig. 33. Solution types in case of $\beta = 0.0111$, $n = 1024$, $t_f = 100$, $A = 4$, labels: 1-Single KdV soliton, 2-KdV soliton ensemble, 3-KdV soliton ensemble with weak tail, 4-soliton with strong tail, 5-solitary wave with tail and wave packet.

6 The behavior of amplitudes of solitons against solution types

In this section the behavior of amplitudes of solitons against solution types is analysed.

In case of the first solution type, i.e., single KdV soliton, the KdV soliton propagates with constant amplitude, see Figs. 34 and 35.

In case of the second solution type, i.e., KdV soliton ensemble, the amplitudes of the higher KdV solitons increase compared with initial amplitude. The elastic interactions of KdV solitons are clearly visible, see Figs. 36 and 37. The number of solitons could be clearly seen from Fig. 36 as there are 2 solitons and in Fig. 37 as there are 8 solitons. See the corresponding time–slice plots in Figs. 5–8.

In case of the third solution type, i.e., KdV soliton with weak tail, the amplitude of the highest KdV soliton increases compared with initial amplitude. The interactions of KdV solitons are visible but additionally the maxima that correspond to the tail are visible near zero level of amplitude, in Figs. 38–39. See the corresponding time–slice plots in Figs. 9–14. The tail causes small variations in the amplitude curves, but does not change the main character of the KdV soliton ensemble – the interactions between the KdV solitons remain (almost) elastic.

In case of the fourth solution type, i.e., KdV soliton with strong tail, the amplitude of the KdV soliton decreases compared with the initial amplitude. In case of the fourth solution type there is always only one (KdV) soliton, which amplitude oscillates about a certain constant level, see Figs. 40–41. See the corresponding time–slice plots Figs. 15–20.

In case of the fifth solution type, i.e., solitary wave with tail and wave packet, the amplitude of the solitary wave strongly oscillates around a certain constant level, that is lower than the amplitude of the initial pulse, see Figs. 42–43. See the corresponding time–slice plots in Figs. 21–26.

In Figs. 44–48 the amplitude changes are presented against α_1 and α_2 : (i) cases where the amplitude decreases are marked as d , (ii) cases where the amplitude increases are marked as u and (iii) cases where the amplitude remains on the initial level are marked as o . If the macrostructure dispersion parameter α_1 and macrostructure parameter α_2 have equal values then amplitude does not change. If $\alpha_1 < \alpha_2$ then amplitude always decreases for all considered values of β . If $\alpha_1 > \alpha_2$ then amplitude increases for $\beta \geq 1.111$ and decreases for $\beta \leq 0.111$.

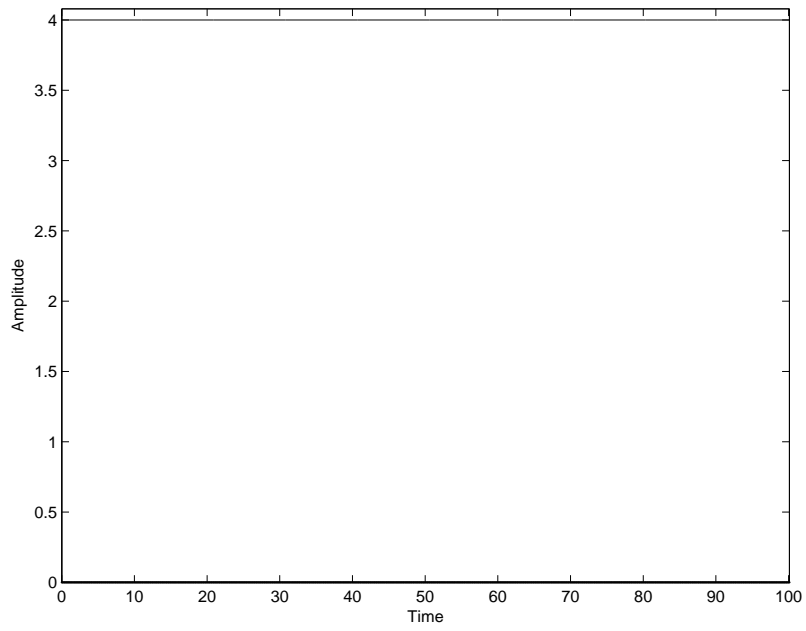


Fig. 34. Single KdV soliton. Soliton amplitude against time in case of $\alpha_1 = 0.07$, $\alpha_2 = 0.07$, $\beta = 11.111$, $n = 1024$, $t_f = 100$, $A = 4$.

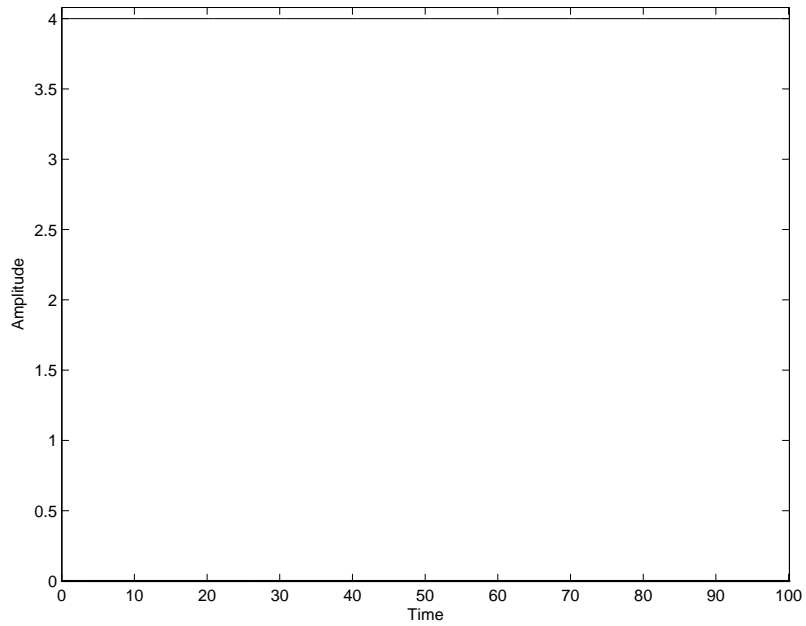


Fig. 35. Single KdV soliton. Soliton amplitude against time in case of $\alpha_1 = 0.01$, $\alpha_2 = 0.01$, $\beta = 111.11$, $n = 1024$, $t_f = 100$, $A = 4$.

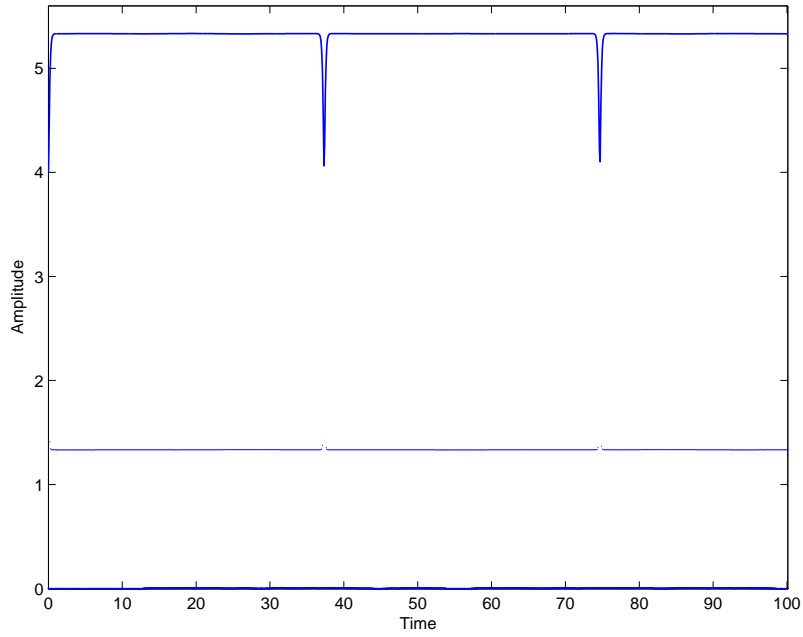


Fig. 36. KdV soliton ensemble. Amplitudes of the wave-profile maxima against time in case of $\alpha_1 = 0.03$, $\alpha_2 = 0.01$, $\beta = 11.111$, $n = 1024$, $t_f = 100$, $A = 4$.

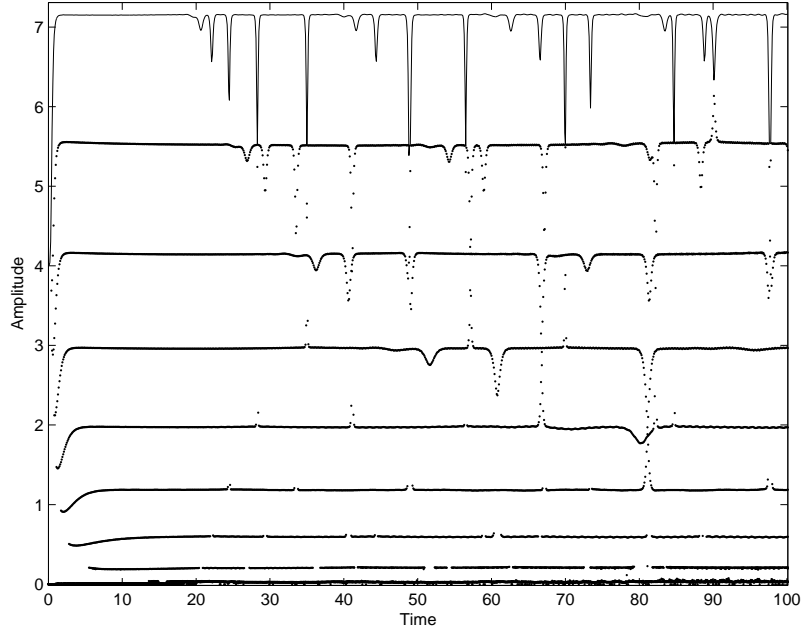


Fig. 37. KdV soliton ensemble. Amplitudes of the wave-profile maxima against time in case of $\alpha_1 = 0.4$, $\alpha_2 = 0.01$, $\beta = 11.11$, $n = 1024$, $t_f = 100$, $A = 4$.

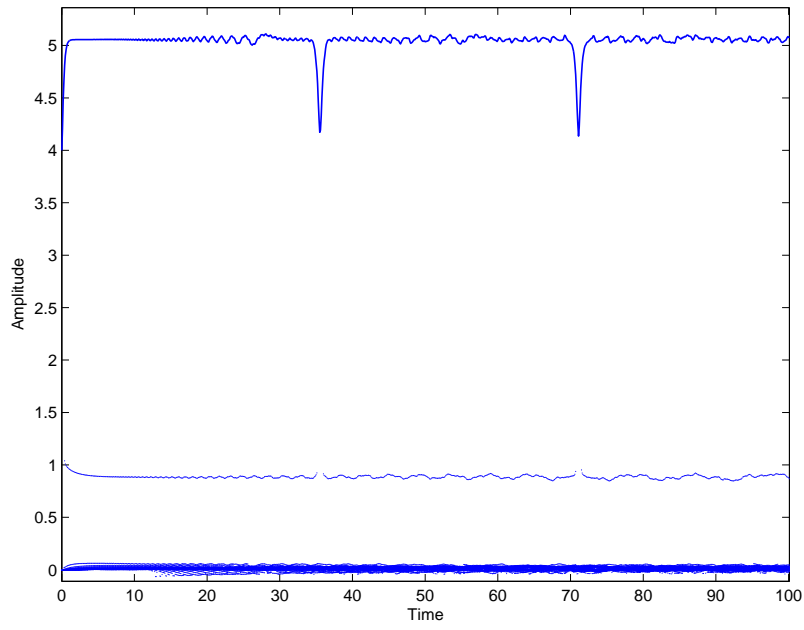


Fig. 38. KdV soliton ensemble with weak tail. Amplitudes of the wave-profile maxima against time in case of $\alpha_1 = 0.07$, $\alpha_2 = 0.03$, $\beta = 11.111$, $n = 1024$, $t_f = 100$, $A = 4$.

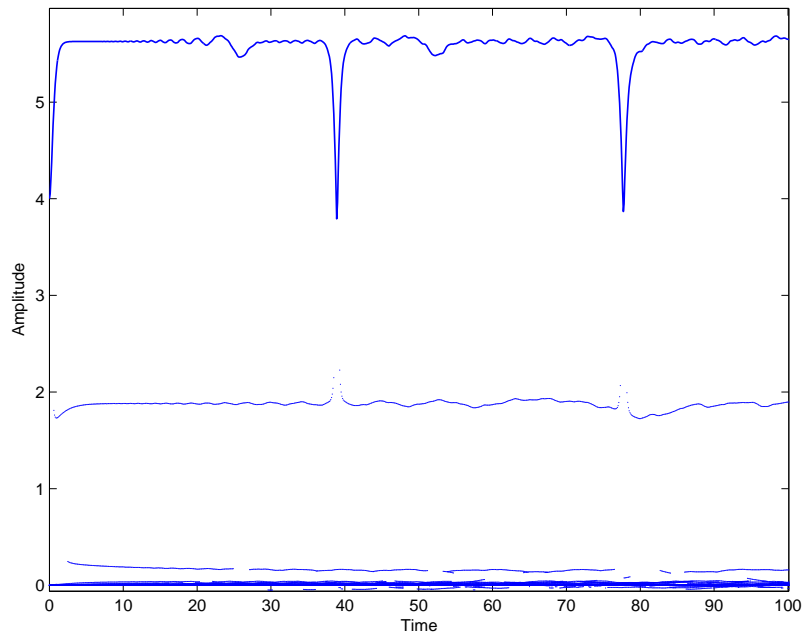


Fig. 39. KdV soliton ensemble with weak tail. Amplitudes of the wave-profile maxima against time in case of $\alpha_1 = 0.4$, $\alpha_2 = 0.1$, $\beta = 111.11$, $n = 1024$, $t_f = 100$, $A = 4$.

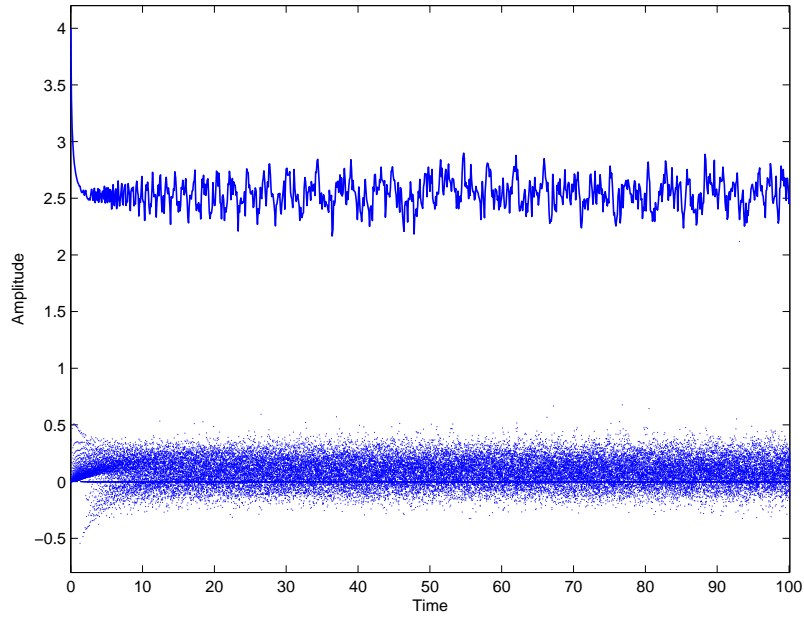


Fig. 40. Soliton with strong tail. Amplitudes of the wave-profile maxima against time in case of $\alpha_1 = 0.03$, $\alpha_2 = 0.09$, $\beta = 11.111$, $n = 1024$, $t_f = 100$, $A = 4$.

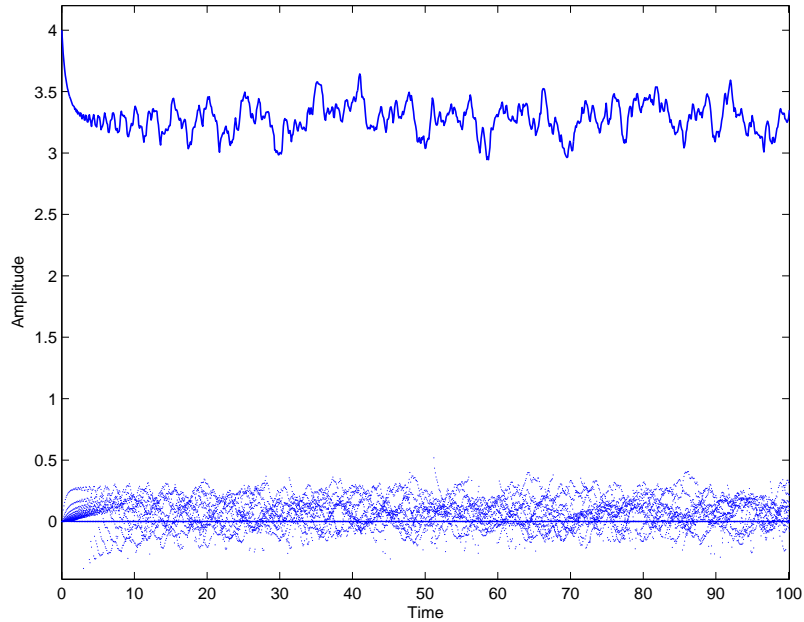


Fig. 41. Soliton with strong tail. Amplitudes of the wave-profile maxima against time in case of $\alpha_1 = 0.4$, $\alpha_2 = 0.7$, $\beta = 111.11$, $n = 1024$, $t_f = 100$, $A = 4$.

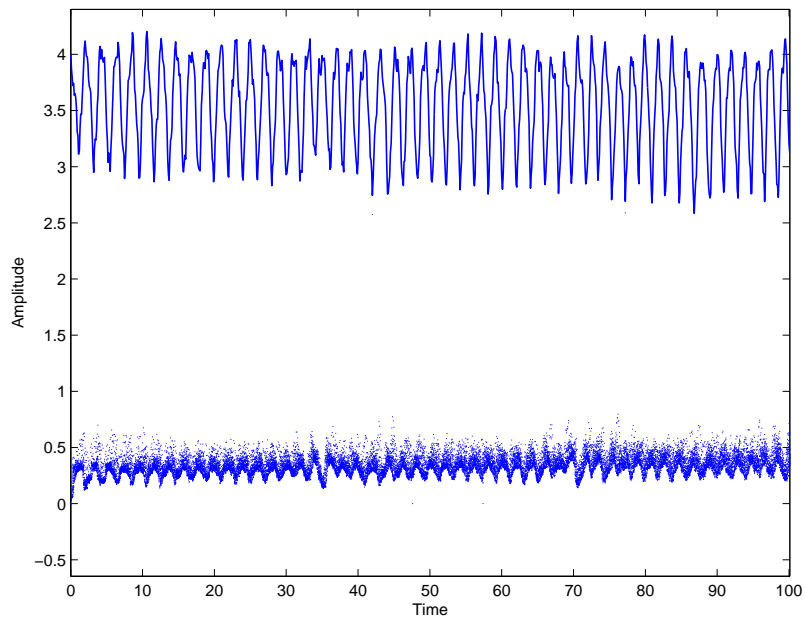


Fig. 42. Solitary wave with tail and wave packet. Amplitudes of the wave-profile maxima against time in case of $\alpha_1 = 0.05$, $\alpha_2 = 0.07$, $\beta = 0.0111$, $n = 1024$, $t_f = 100$, $A = 4$.

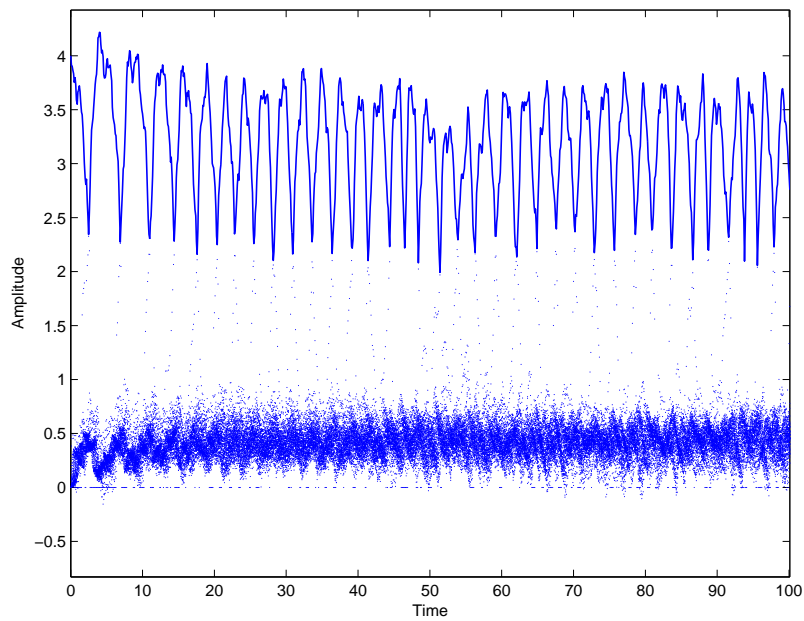


Fig. 43. Solitary wave with tail and wave packet. Amplitudes of the wave-profile maxima against time in case of $\alpha_1 = 0.07$, $\alpha_2 = 0.11$, $\beta = 0.0111$, $n = 1024$, $t_f = 100$, $A = 4$.

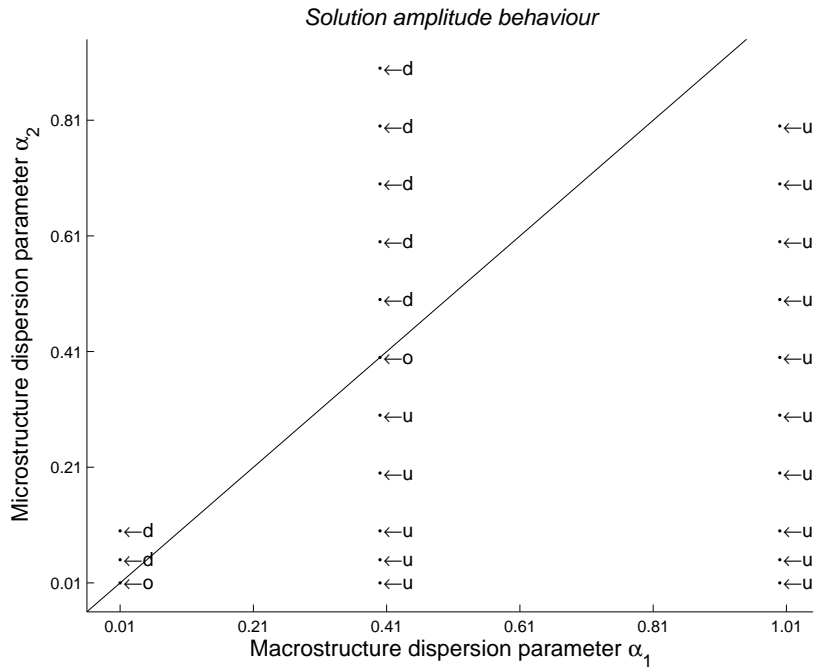


Fig. 44. Amplitude behavior compared to initial amplitude in case of $\beta = 111.11$, $n = 1024$, $t_f = 100$, $A = 4$, labels: d - down, u - up, o - no change.

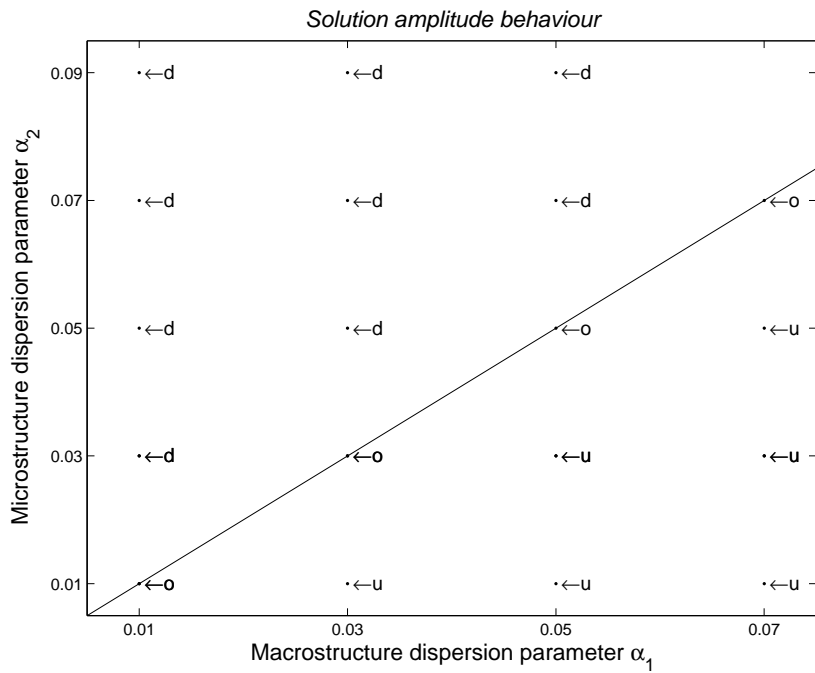


Fig. 45. Amplitude behavior compared to initial amplitude in case of $\beta = 11.111$, $n = 1024$, $t_f = 100$, $A = 4$, labels: d - down, u - up, o - no change.

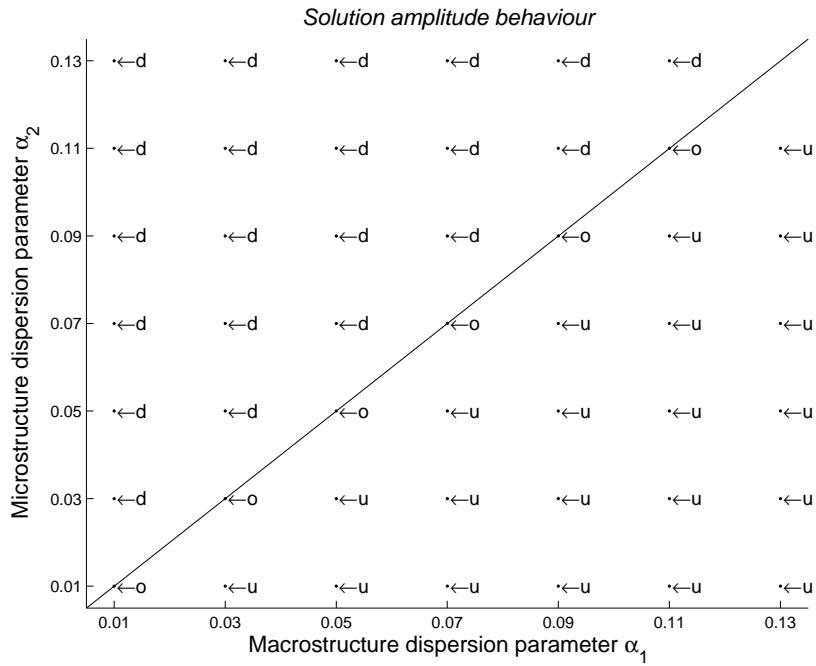


Fig. 46. Amplitude behavior compared to initial amplitude in case of $\beta = 1.111$, $n = 1024$, $t_f = 100$, $A = 4$, labels: d - down, u - up, o - no change.

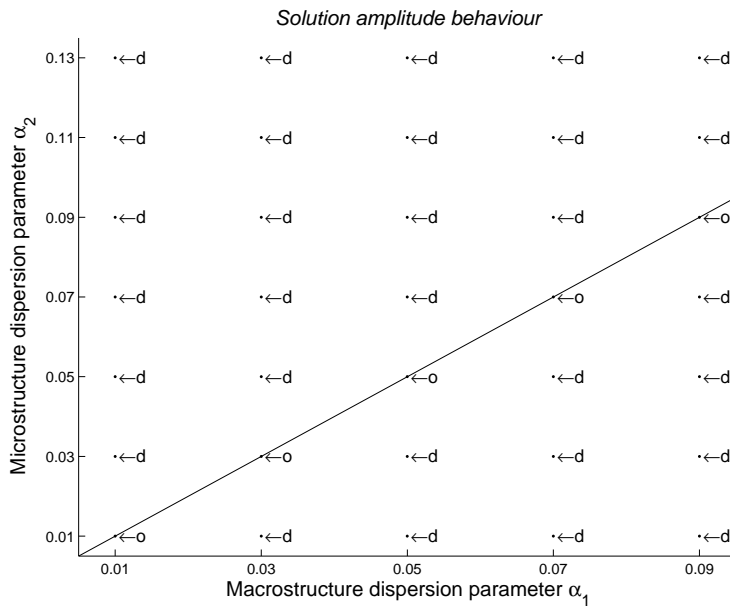


Fig. 47. Amplitude behavior compared to initial amplitude in case of $\beta = 0.1111$, $n = 1024$, $t_f = 100$, $A = 4$, labels: d - down, u - up, o - no change.

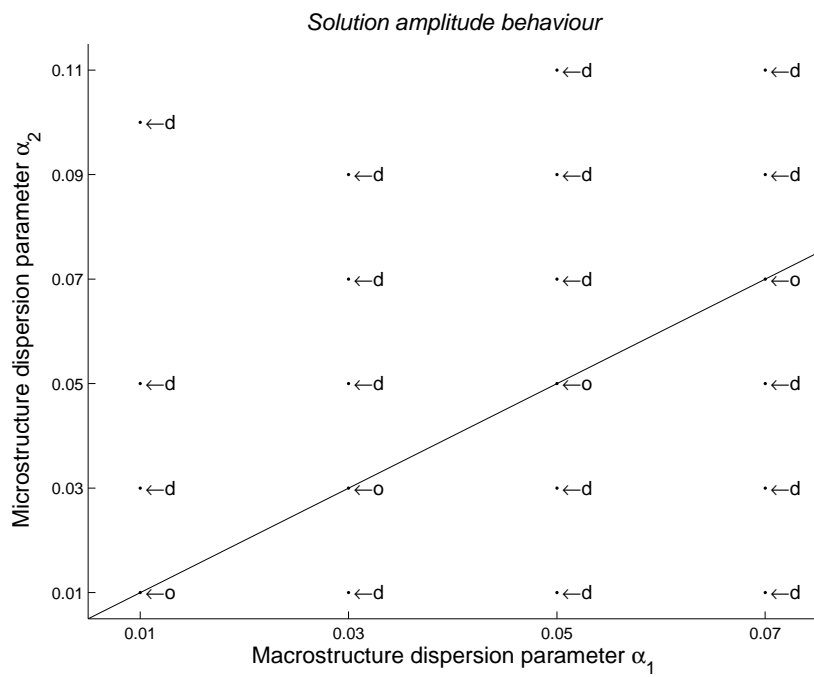


Fig. 48. Amplitude behavior compared to initial amplitude in case of $\beta = 0.0111$, $n = 1024$, $t_f = 100$, $A = 4$, labels: d - down, u - up, o - no change.

7 Number of KdV solitons

In Figs. 49–53 the number of solitons are presented against the dispersion parameters α_1 and α_2 for different values of microstructure parameter β .

In case of $\alpha_1 \leq \alpha_2$ there is always only one soliton. In case of $\beta \geq 1.111$ and $\alpha_1 > \alpha_2$ the number of solitons in the KdV ensemble increases step by step, if α_1 increases and α_2 is fixed or if α_2 decreases and α_1 is fixed, see Figs. 49–51.

For $\beta \leq 0.1111$ the number of solitons is one for $\alpha_1 > \alpha_2$, see Figs. 52–53.

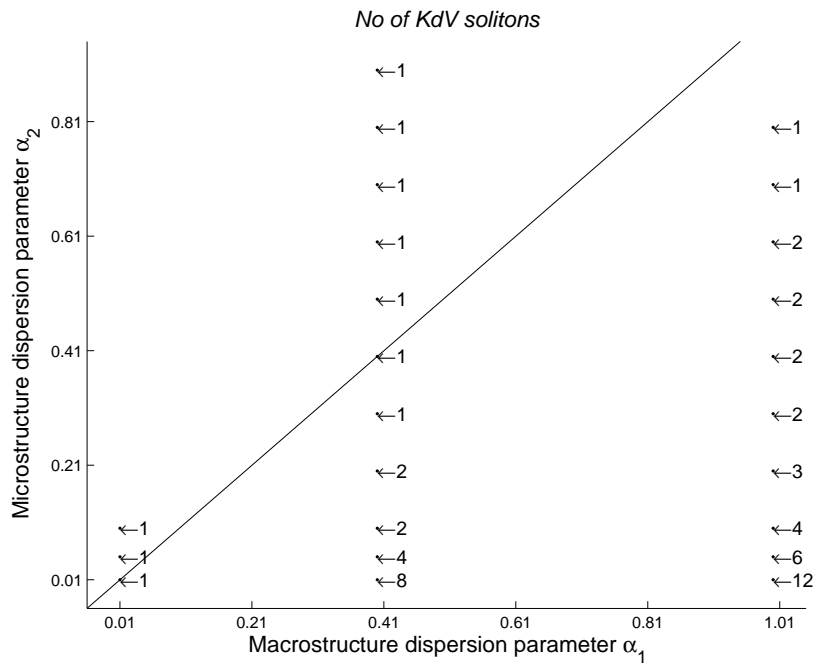


Fig. 49. No of KdV solitons in case of $\beta = 111.11$, $n = 1024$, $t_f = 100$, $A = 4$.

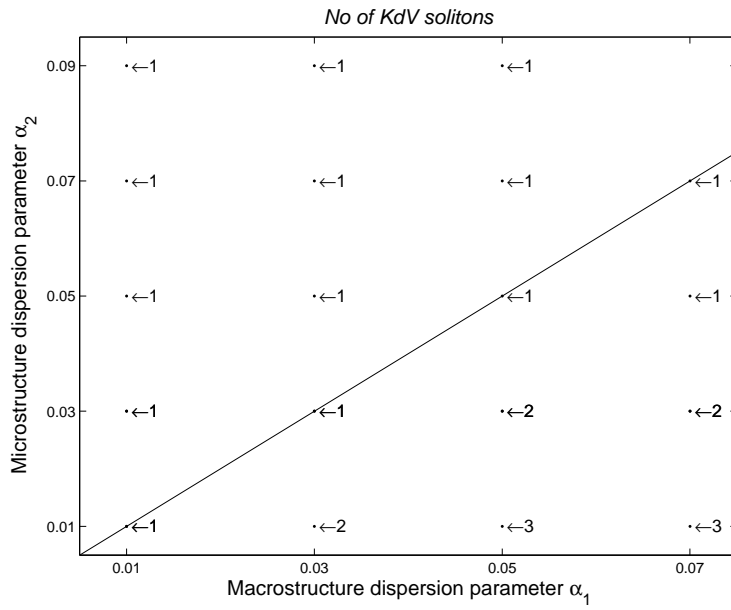


Fig. 50. No of KdV solitons in case of $\beta = 11.111$, $n = 1024$, $t_f = 100$, $A = 4$.

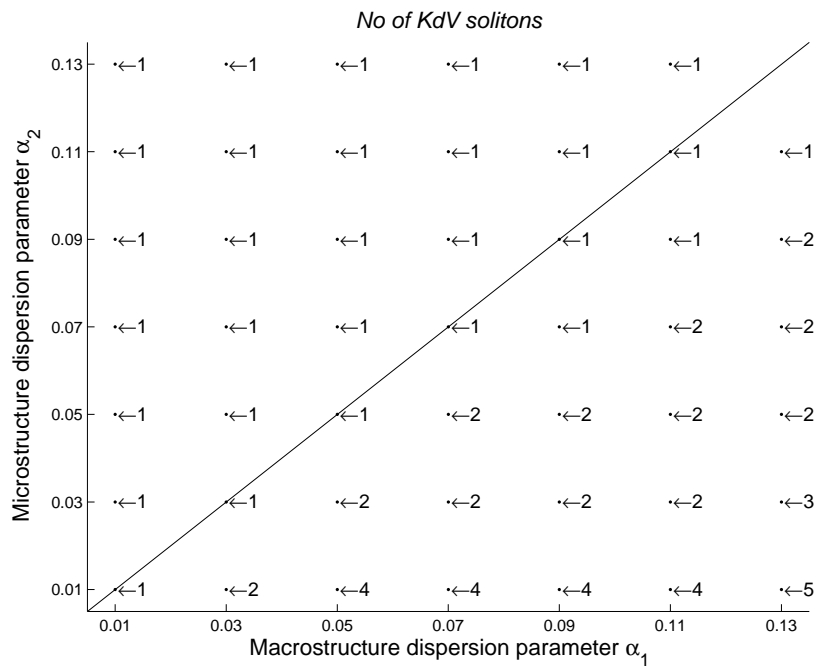


Fig. 51. No of KdV solitons in case of $\beta = 1.111$, $n = 1024$, $t_f = 100$, $A = 4$.

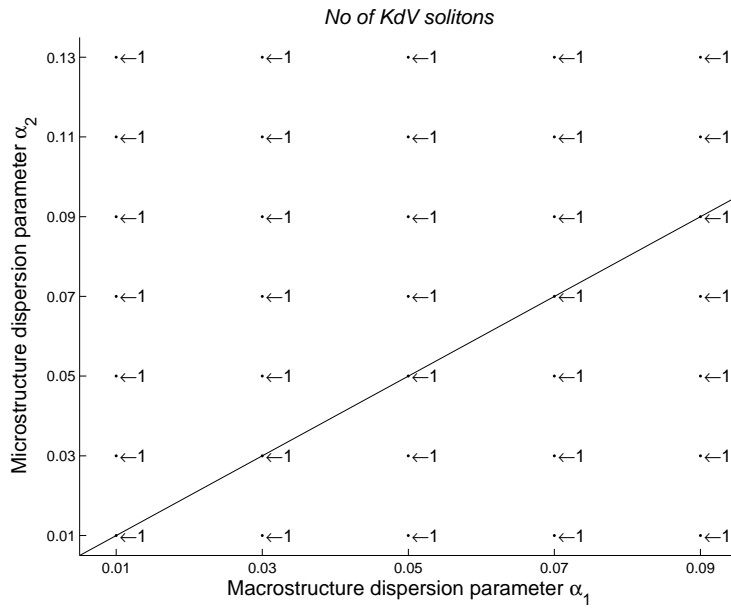


Fig. 52. No of KdV solitons in case of $\beta = 0.1111$, $n = 1024$, $t_f = 100$, $A = 4$.

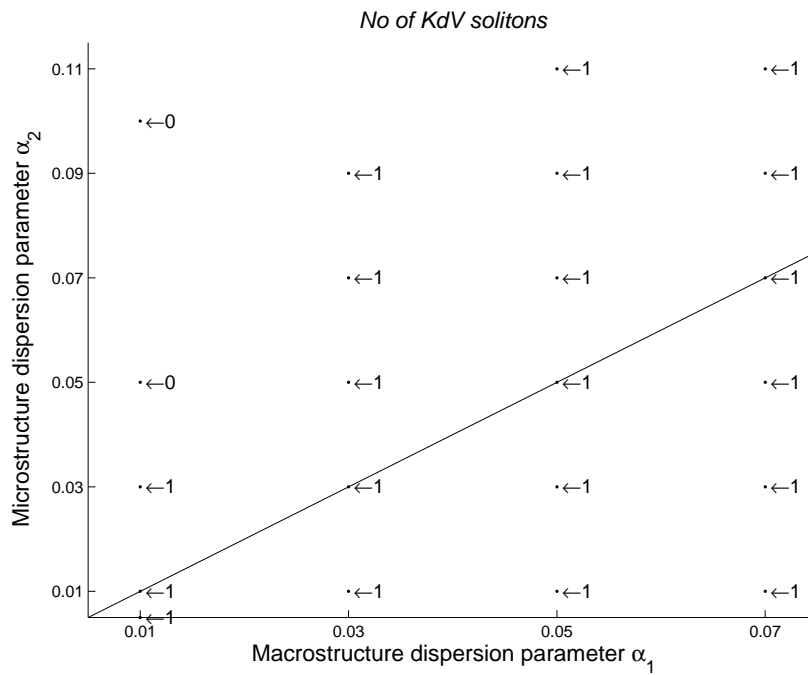


Fig. 53. No of KdV solitons in case of $\beta = 0.0111$, $n = 1024$, $t_f = 100$, $A = 4$.

8 The influence of initial amplitude

In this section the influence of the initial amplitude on the solutions behavior is described and analysed. In Figs. 54–86 different solutions with different values of parameters α_1 , α_2 , β and A are presented.

In case of the first solution type the increase of initial amplitude from $A = 1$ to $A = 10$ causes the increase in the propagation speed of the KdV soliton. The essence of the solution remains the same for all three values of amplitude A . See the corresponding pseudocolor plots in Figs. 54–56.

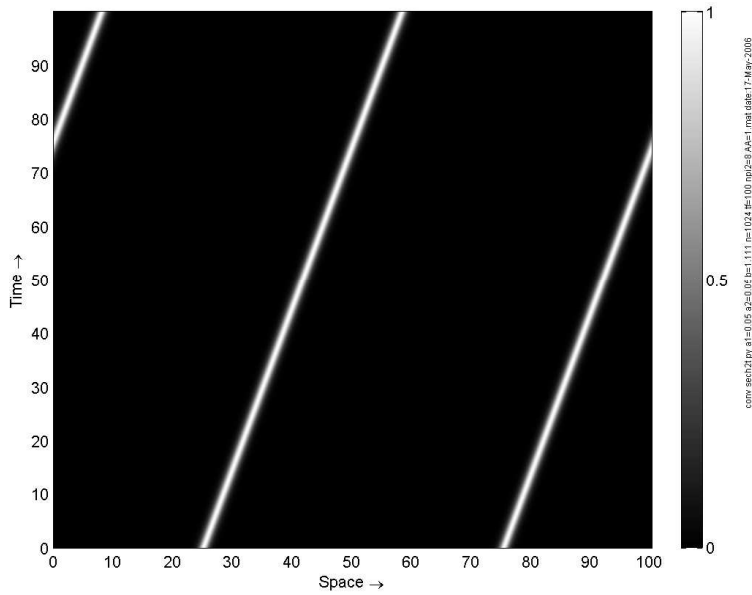


Fig. 54. Pseudocolor plot over two space periods for $\alpha_1 = 0.05$, $\alpha_2 = 0.05$, $\beta = 1.111$, $n = 1024$, $t_f = 100$, $A = 1$

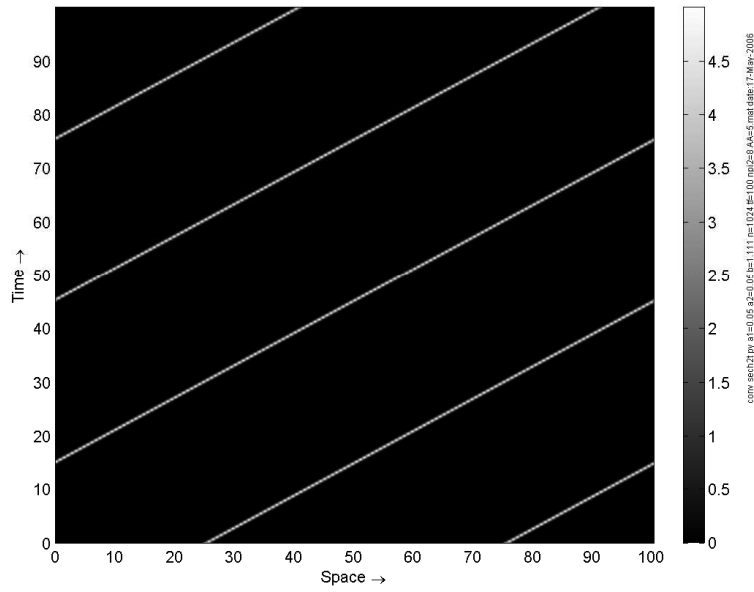


Fig. 55. Pseudocolor plot over two space periods for $\alpha_1 = 0.05$, $\alpha_2 = 0.05$, $\beta = 1.111$, $n = 1024$, $t_f = 100$, $A = 5$

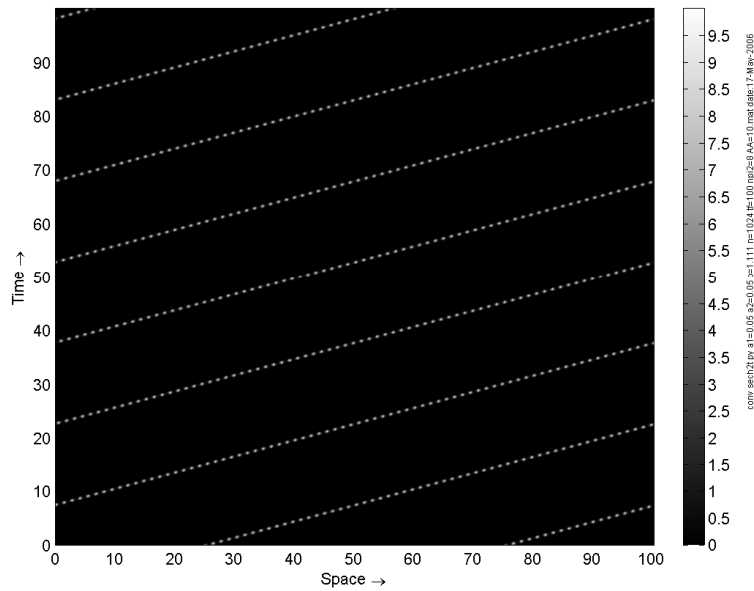


Fig. 56. Pseudocolor plot over two space periods for $\alpha_1 = 0.05$, $\alpha_2 = 0.05$, $\beta = 1.111$, $n = 1024$, $t_f = 100$, $A = 10$

In case of the second solution type the increase of the initial amplitude from $A = 1$ to $A = 10$ causes the increase of the propagation speed of solitons in the KdV soliton ensemble but the number of solitons does not change. See corresponding pseudocolor plots in Figs. 57, 59, 61 and amplitude curves in Figs. 58, 60, 62.

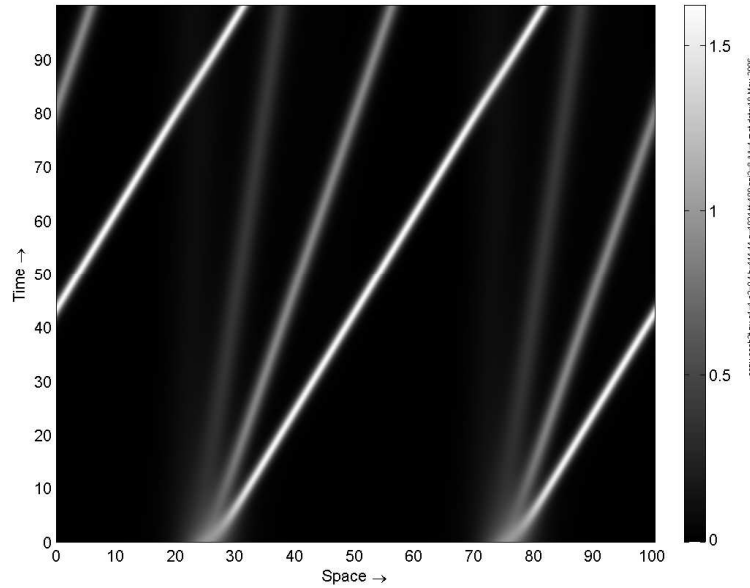


Fig. 57. KdV soliton ensemble. Pseudocolor plot over two space periods for $\alpha_1 = 1$, $\alpha_2 = 0.1$, $\beta = 111.11$, $n = 1024$, $t_f = 100$, $A = 1$.

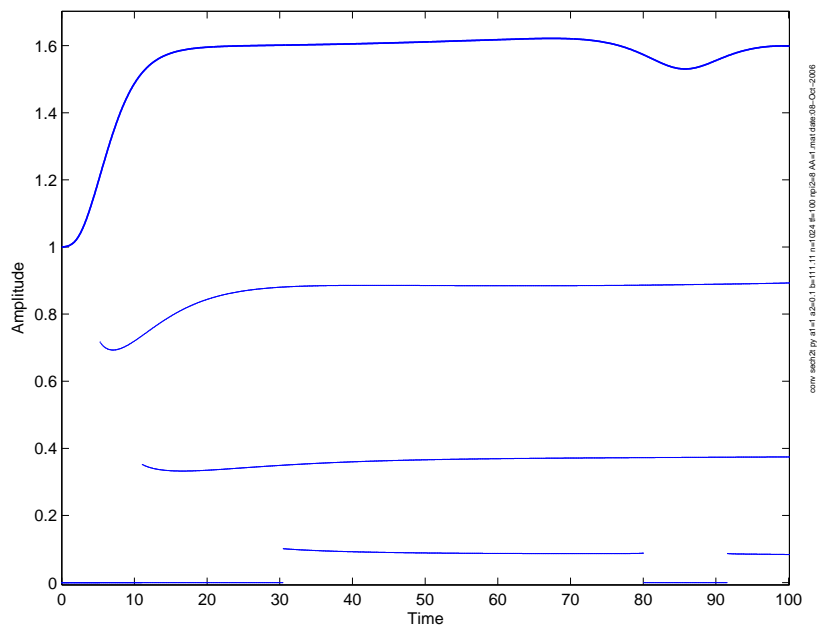


Fig. 58. KdV soliton ensemble. Amplitudes of the wave-profile maxima against time in case of $\alpha_1 = 1$, $\alpha_2 = 0.1$, $\beta = 111.11$, $n = 1024$, $t_f = 100$, $A = 1$.

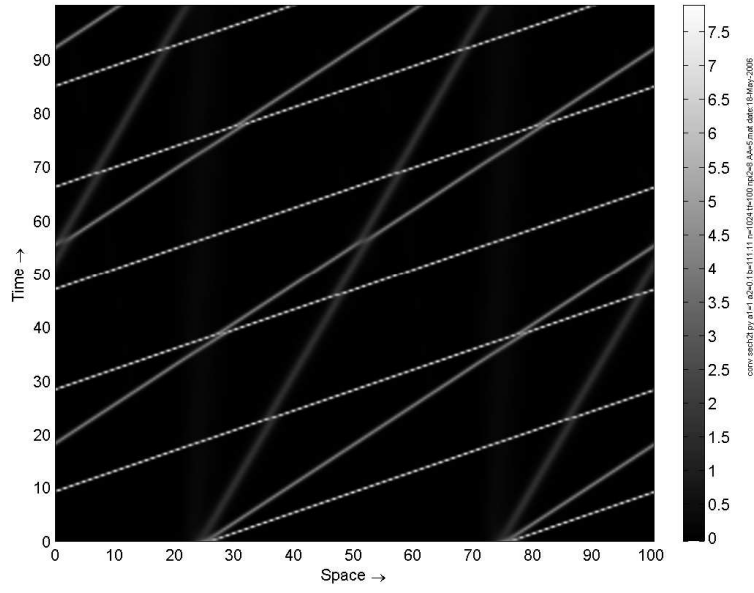


Fig. 59. KdV soliton ensemble. Pseudocolor plot over two space periods for $\alpha_1 = 1$, $\alpha_2 = 0.1$, $\beta = 111.11$, $n = 1024$, $t_f = 100$, $A = 5$.

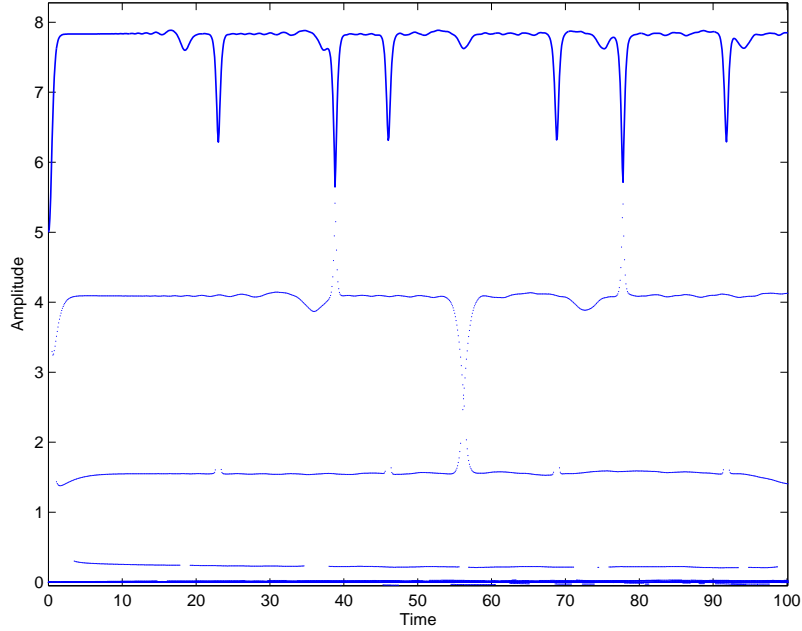


Fig. 60. KdV soliton ensemble. Amplitudes of the wave-profile maxima against time in case of $\alpha_1 = 1$, $\alpha_2 = 0.1$, $\beta = 111.11$, $n = 1024$, $t_f = 100$, $A = 5$.

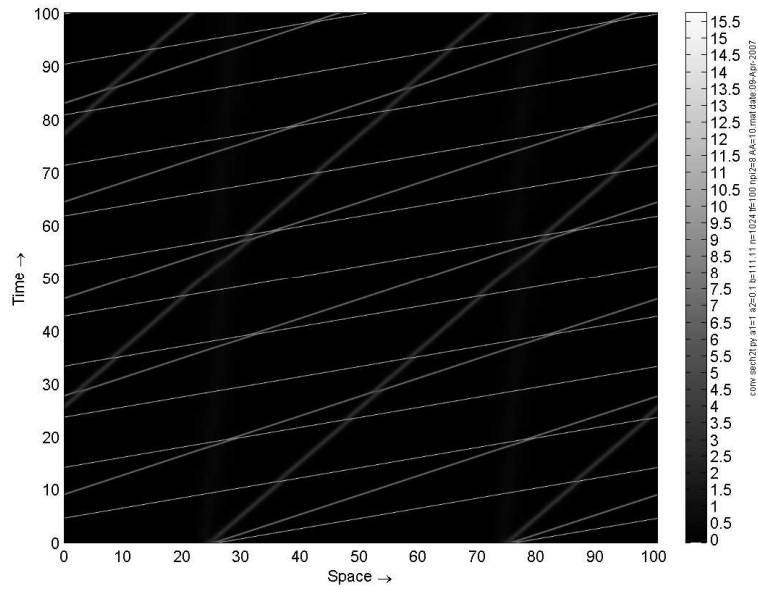


Fig. 61. KdV soliton ensemble. Pseudocolor plot over two space periods for $\alpha_1 = 1$, $\alpha_2 = 0.1$, $\beta = 111.11$, $n = 1024$, $t_f = 100$, $A = 10$.

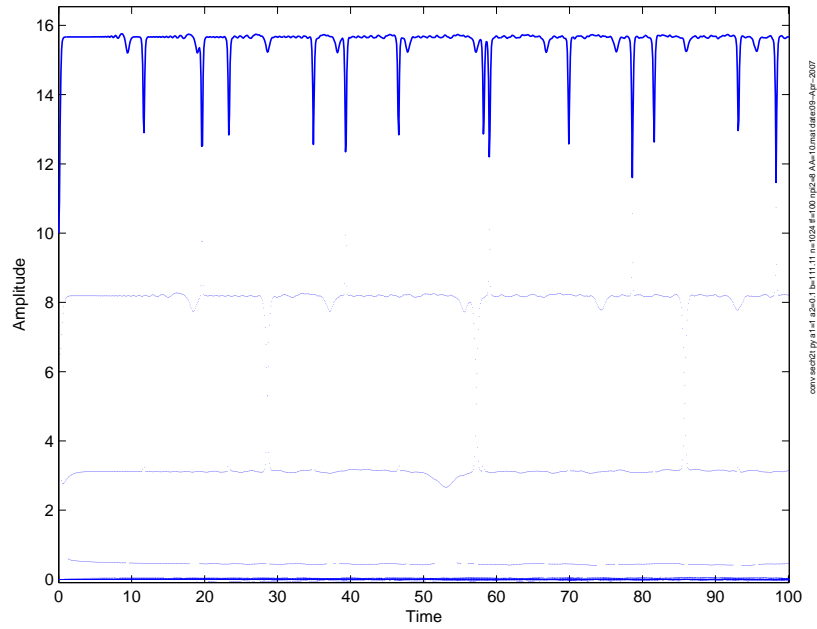


Fig. 62. KdV soliton ensemble. Amplitudes of the wave-profile maxima against time in case of $\alpha_1 = 1$, $\alpha_2 = 0.1$, $\beta = 111.11$, $n = 1024$, $t_f = 100$, $A = 10$.

In case of the third solution type the increase of the initial amplitude causes the increase of propagation speed of KdV solitons. The essence of the solution remains the same for all values of amplitude $A = 1, 5, 10, 15$. The amplitude of the weak tail increases if the initial amplitude increases but it does not alter the solution type. See the corresponding pseudocolor plots in Figs. 63, 65, 67, 69 and the amplitude curves in Figs. 64, 66, 68, 70.

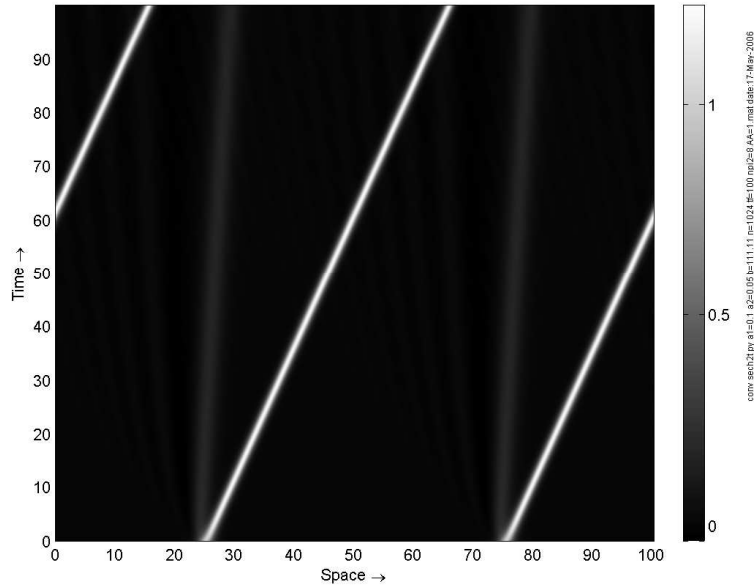


Fig. 63. KdV soliton ensemble with weak tail. Pseudocolor plot over two space periods for $\alpha_1 = 0.1$, $\alpha_2 = 0.05$, $\beta = 111.11$, $n = 1024$, $t_f = 100$, $A = 1$.

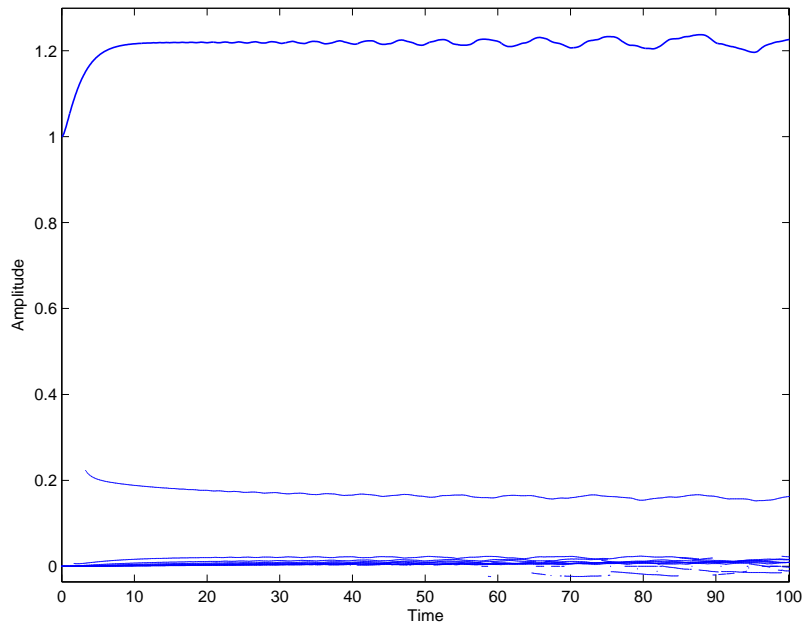


Fig. 64. KdV soliton ensemble with weak tail. Amplitudes of the wave-profile maxima against time in case of $\alpha_1 = 0.1$, $\alpha_2 = 0.05$, $\beta = 111.11$, $n = 1024$, $t_f = 100$, $A = 1$.

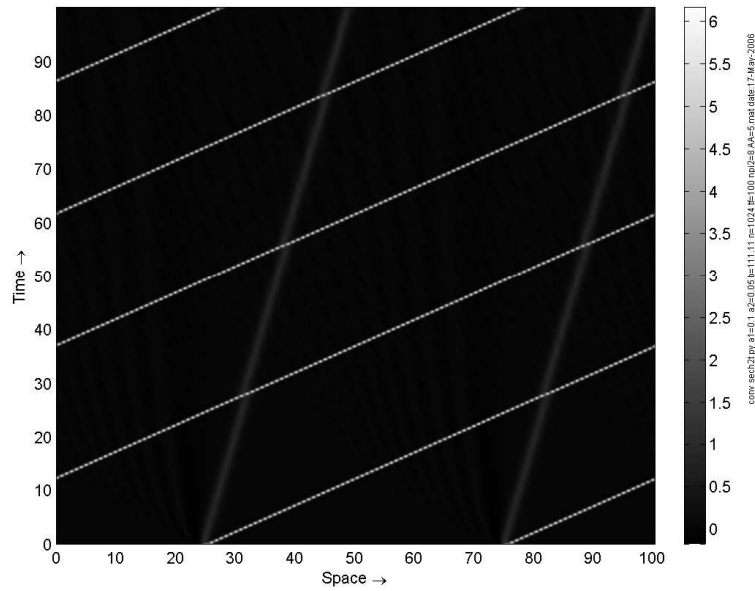


Fig. 65. KdV soliton ensemble with weak tail. Pseudocolor plot over two space periods for $\alpha_1 = 0.1$, $\alpha_2 = 0.05$, $\beta = 111.11$, $n = 1024$, $t_f = 100$, $A = 5$.

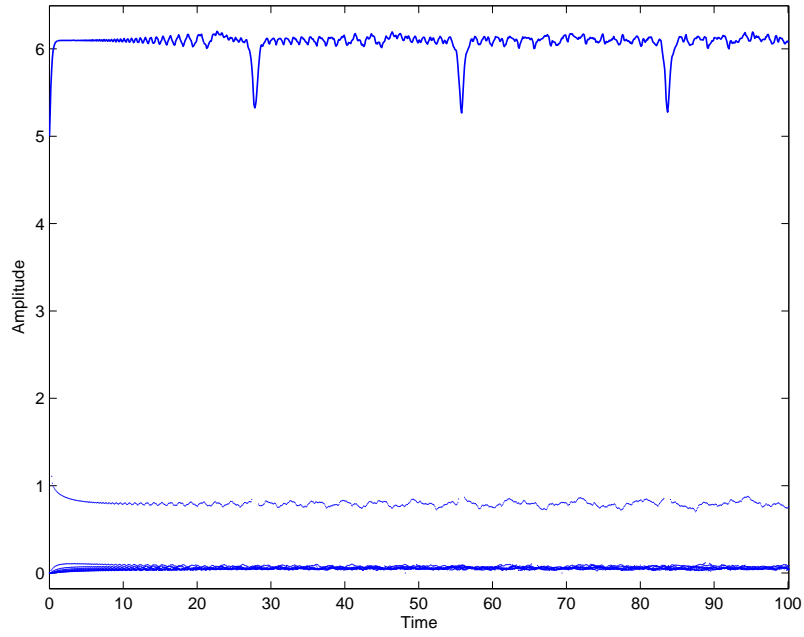


Fig. 66. KdV soliton ensemble with weak tail. Amplitudes of the wave-profile maxima against time in case of $\alpha_1 = 0.1$, $\alpha_2 = 0.05$, $\beta = 111.11$, $n = 1024$, $t_f = 100$, $A = 5$.

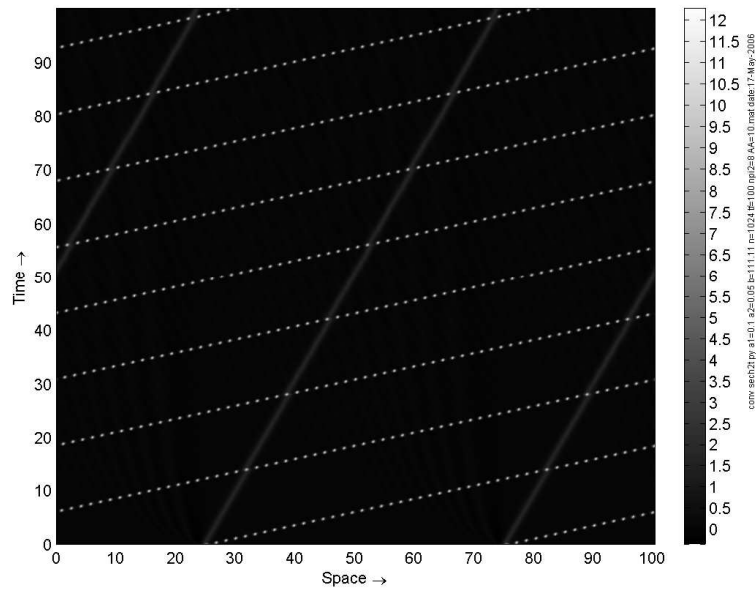


Fig. 67. KdV soliton ensemble with weak tail. Pseudocolor plot over two space periods for $\alpha_1 = 0.1$, $\alpha_2 = 0.05$, $\beta = 111.11$, $n = 1024$, $t_f = 100$, $A = 10$.

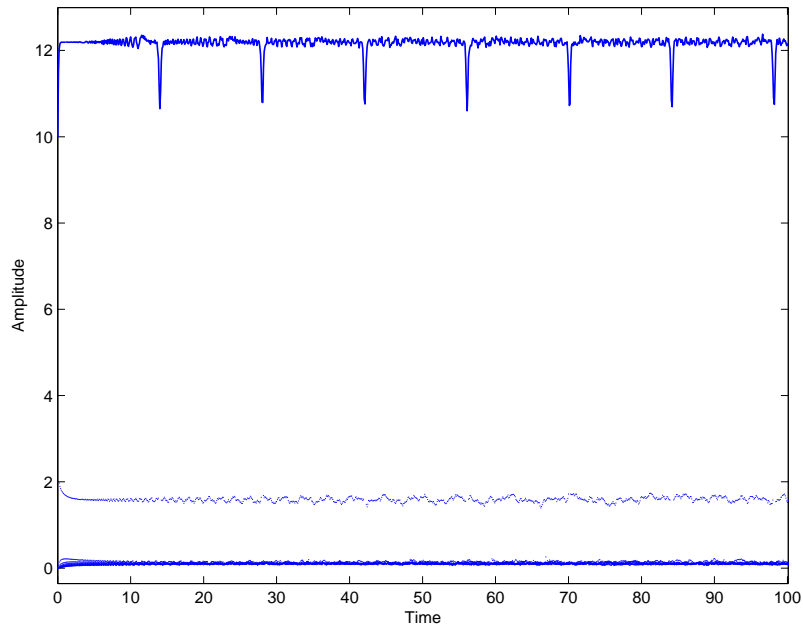


Fig. 68. KdV soliton ensemble with weak tail. Amplitudes of the wave-profile maxima against time in case of $\alpha_1 = 0.1$, $\alpha_2 = 0.05$, $\beta = 111.11$, $n = 1024$, $t_f = 100$, $A = 10$.

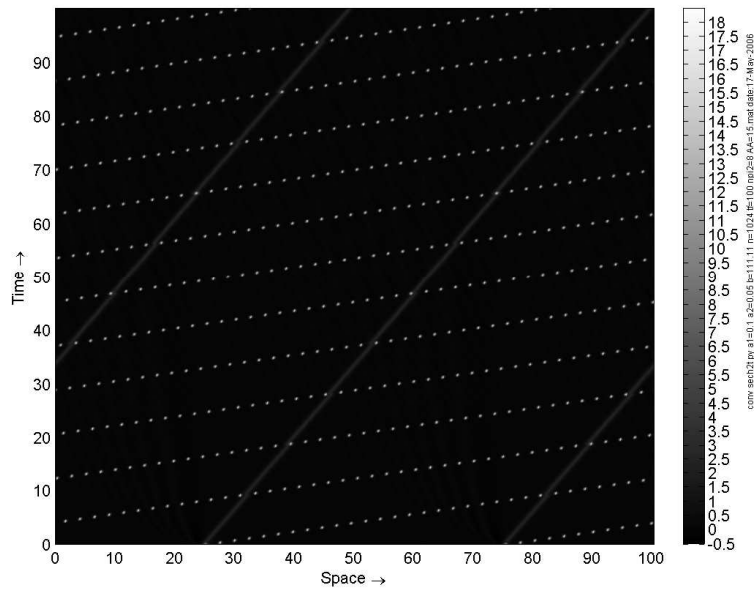


Fig. 69. KdV soliton ensemble with weak tail. Pseudocolor plot over two space periods for $\alpha_1 = 0.1$, $\alpha_2 = 0.05$, $\beta = 111.11$, $n = 1024$, $t_f = 100$, $A = 15$

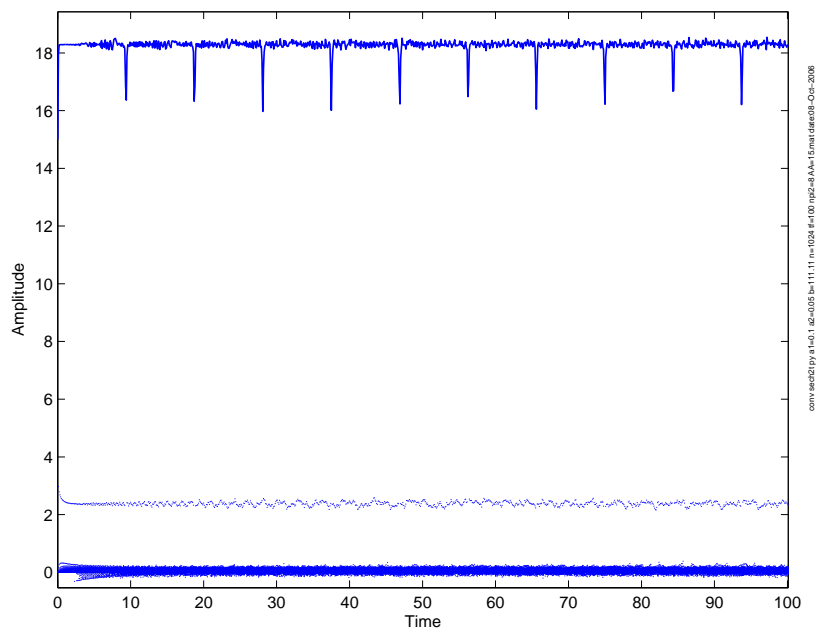


Fig. 70. KdV soliton ensemble with weak tail. Amplitudes of the wave-profile maxima against time in case of $\alpha_1 = 0.1$, $\alpha_2 = 0.05$, $\beta = 111.11$, $n = 1024$, $t_f = 100$, $A = 15$.

In case of the fourth solution type the increase of the initial amplitude from $A = 1$ to $A = 15$ causes the increase of the propagation speed of the soliton similarly to the third solution type. See the corresponding pseudocolor plots in Figs. 71, 73, 75, 77 and the amplitude curves in Figs. 72, 74, 76, 78.

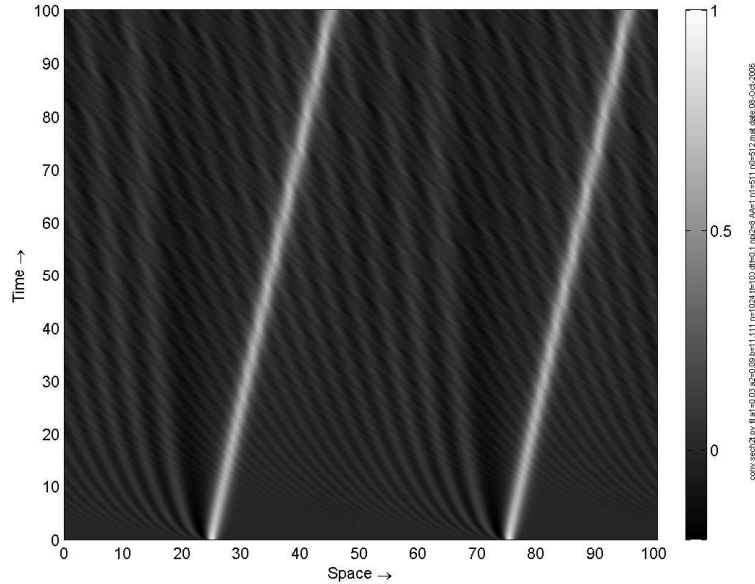
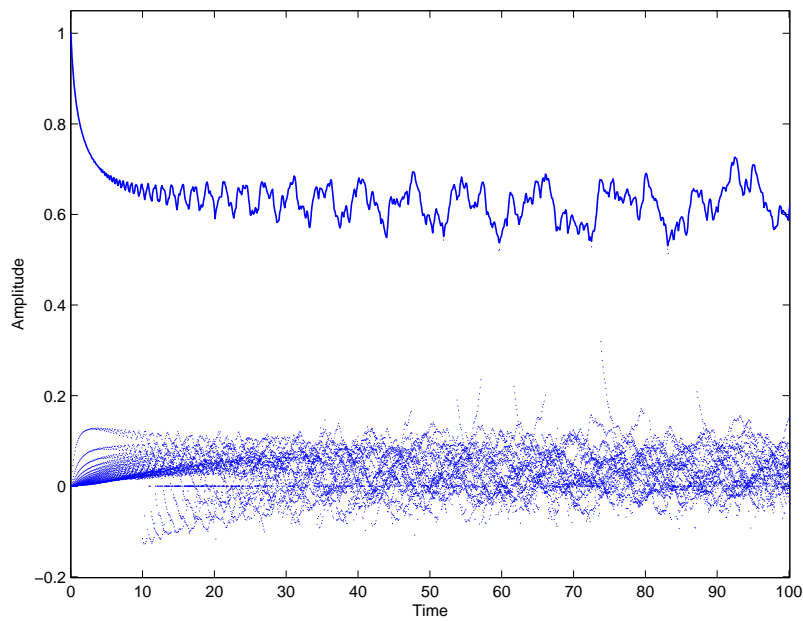


Fig. 71. Soliton with strong tail. Pseudocolor plot over two space periods for $\alpha_1 = 0.03$, $\alpha_2 = 0.09$, $\beta = 11.111$, $n = 1024$, $t_f = 100$, $A = 1$.



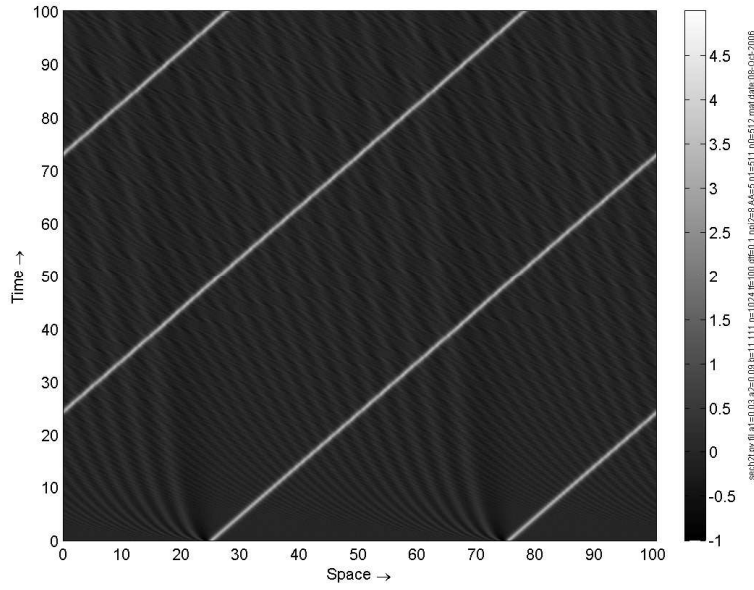


Fig. 73. Soliton with strong tail. Pseudocolor plot over two space periods for $\alpha_1 = 0.03$, $\alpha_2 = 0.09$, $\beta = 11.111$, $n = 1024$, $t_f = 100$, $A = 5$.

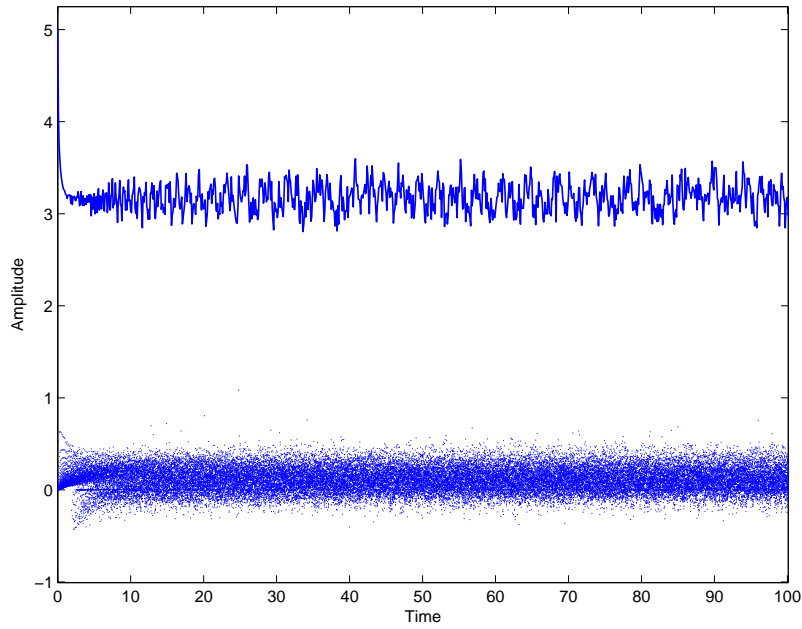


Fig. 74. Soliton with strong tail. Amplitudes of the wave-profile maxima against time in case of $\alpha_1 = 0.03$, $\alpha_2 = 0.09$, $\beta = 11.111$, $n = 1024$, $t_f = 100$, $A = 5$.

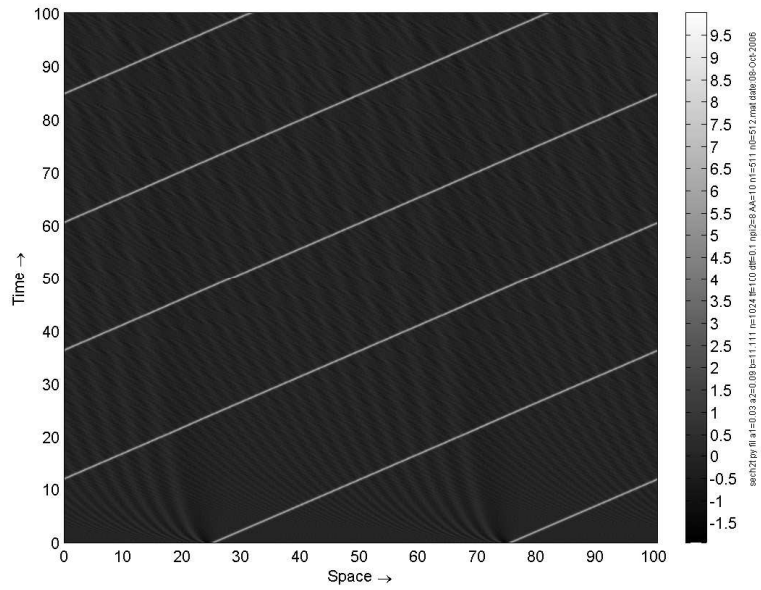


Fig. 75. Soliton with strong tail. Pseudocolor plot over two space periods for $\alpha_1 = 0.03$, $\alpha_2 = 0.09$, $\beta = 11.111$, $n = 1024$, $t_f = 100$, $A = 10$.

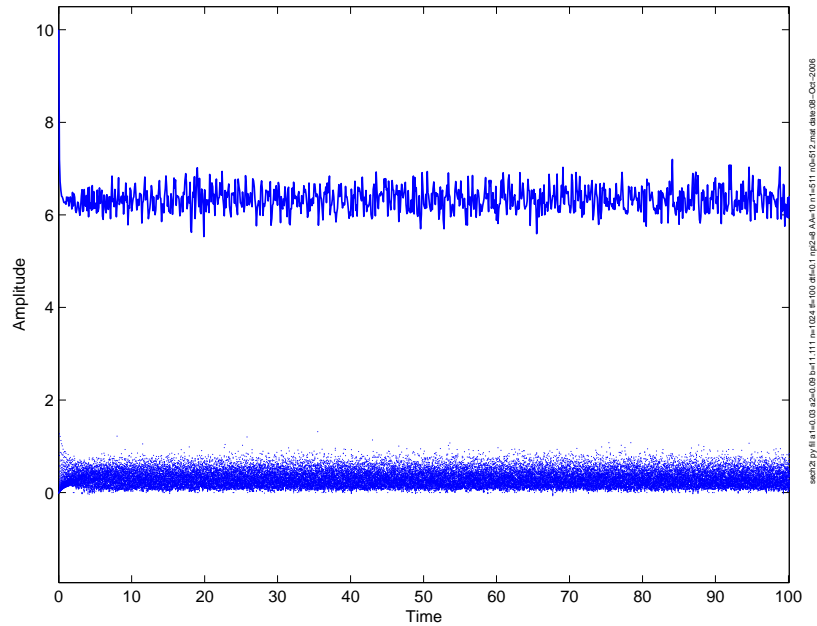


Fig. 76. Soliton with strong tail. Amplitudes of the wave-profile maxima against time in case of $\alpha_1 = 0.03$, $\alpha_2 = 0.09$, $\beta = 11.111$, $n = 1024$, $t_f = 100$, $A = 10$.

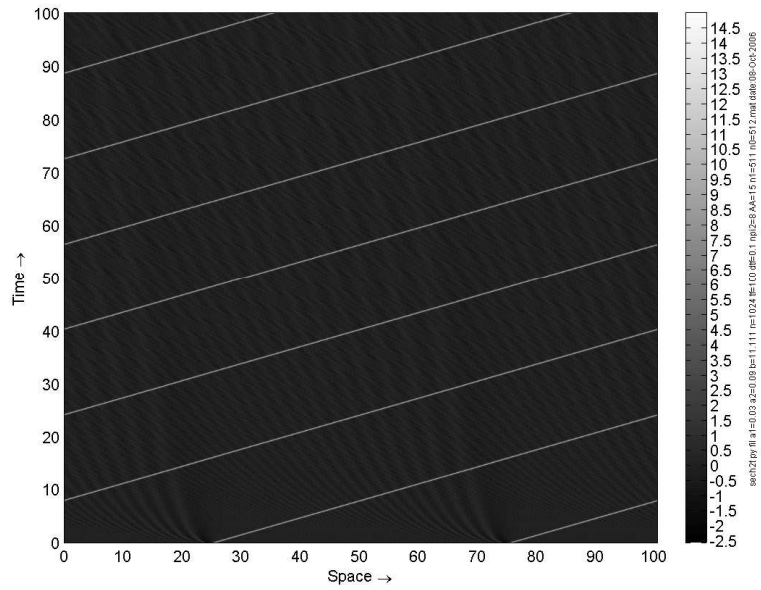


Fig. 77. Soliton with strong tail. Pseudocolor plot over two space periods for $\alpha_1 = 0.03$, $\alpha_2 = 0.09$, $\beta = 11.111$, $n = 1024$, $t_f = 100$, $A = 15$.

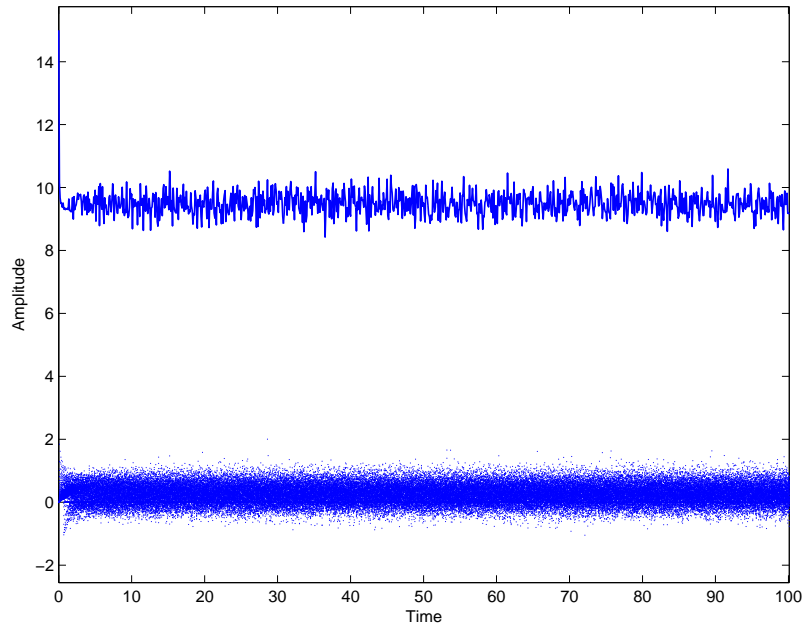


Fig. 78. KdV soliton with strong tail. Amplitudes of the wave-profile maxima against time in case of $\alpha_1 = 0.03$, $\alpha_2 = 0.09$, $\beta = 11.111$, $n = 1024$, $t_f = 100$, $A = 15$.

In case of the fifth solution type the increase of initial amplitude from $A = 1$ to $A = 15$ causes more complex changes than in previous cases — propagation speed of the solitary wave as well as the shape of its trajectory is altered, see Figs. 23, 42, 79–86. However, the solution type does not change.

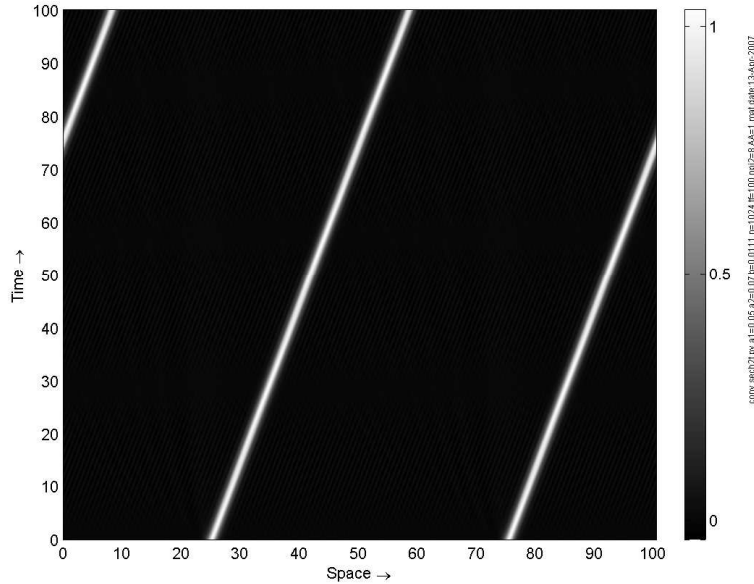


Fig. 79. Solitary wave with tail and wave packet. Pseudocolor plot over two space periods for $\alpha_1 = 0.05$, $\alpha_2 = 0.07$, $\beta = 0.0111$, $n = 1024$, $t_f = 100$, $A = 1$.

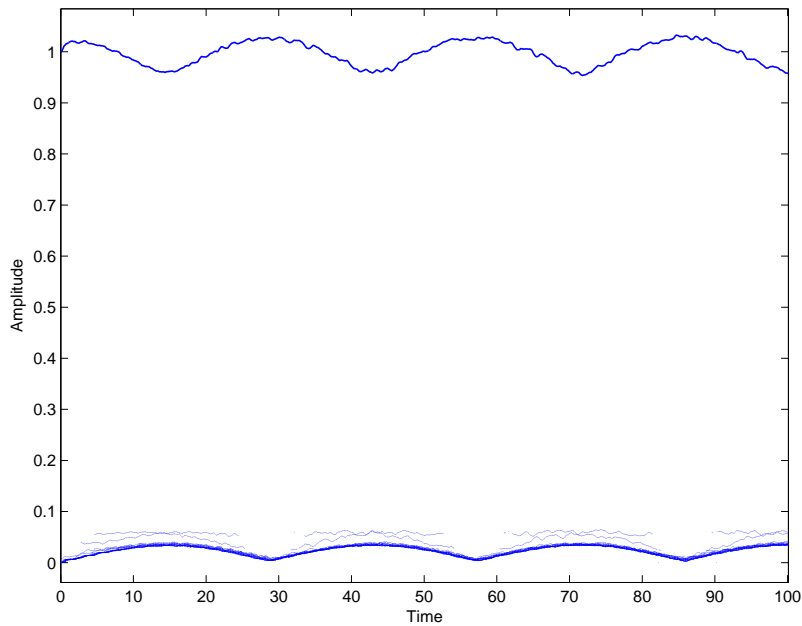


Fig. 80. Solitary wave with tail and wave packet. Amplitudes of the wave-profile maxima against time in case of $\alpha_1 = 0.05$, $\alpha_2 = 0.07$, $\beta = 0.0111$, $n = 1024$, $t_f = 100$, $A = 1$.

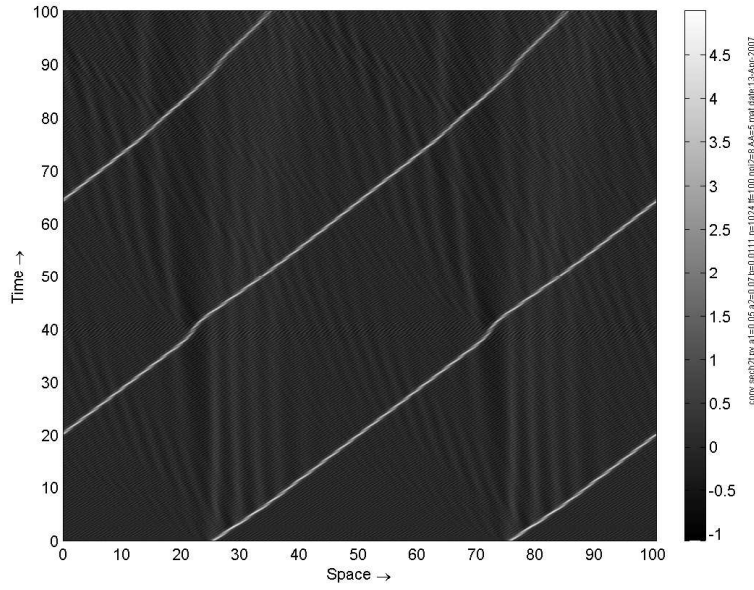


Fig. 81. Solitary wave with tail and wave packet. Pseudocolor plot over two space periods for $\alpha_1 = 0.05$, $\alpha_2 = 0.07$, $\beta = 0.0111$, $n = 1024$, $t_f = 100$, $A = 5$.

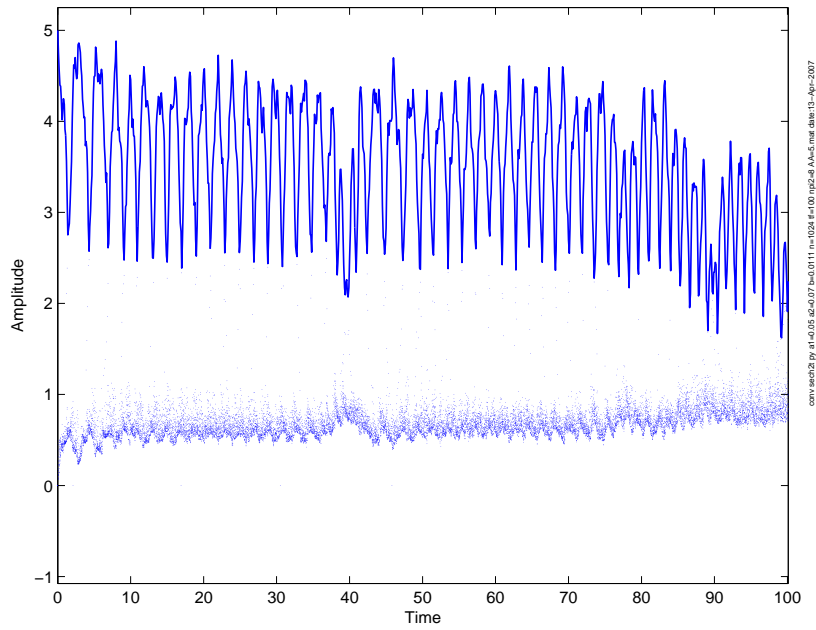


Fig. 82. Solitary wave with tail and wave packet. Amplitudes of the wave-profile maxima against time in case of $\alpha_1 = 0.05$, $\alpha_2 = 0.07$, $\beta = 0.0111$, $n = 1024$, $t_f = 100$, $A = 5$.

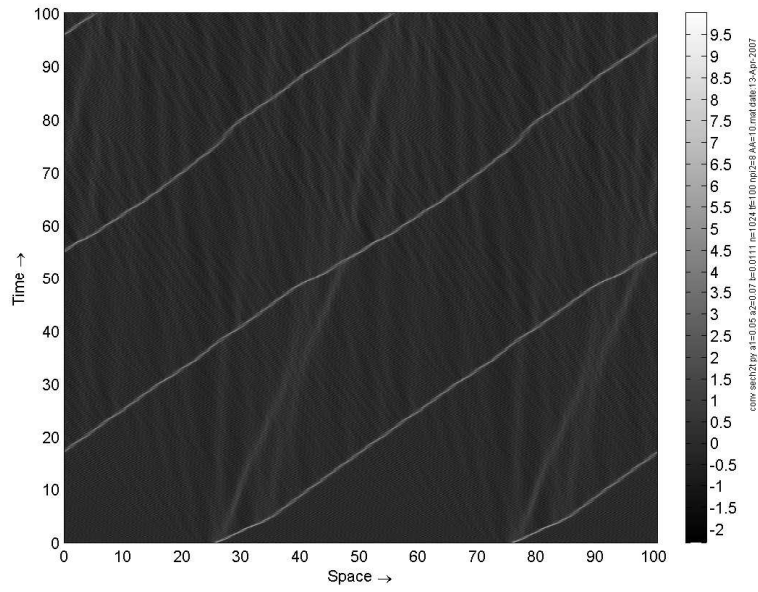


Fig. 83. Solitary wave with tail and wave packet. Pseudocolor plot over two space periods for $\alpha_1 = 0.05$, $\alpha_2 = 0.07$, $\beta = 0.0111$, $n = 1024$, $t_f = 100$, $A = 10$.

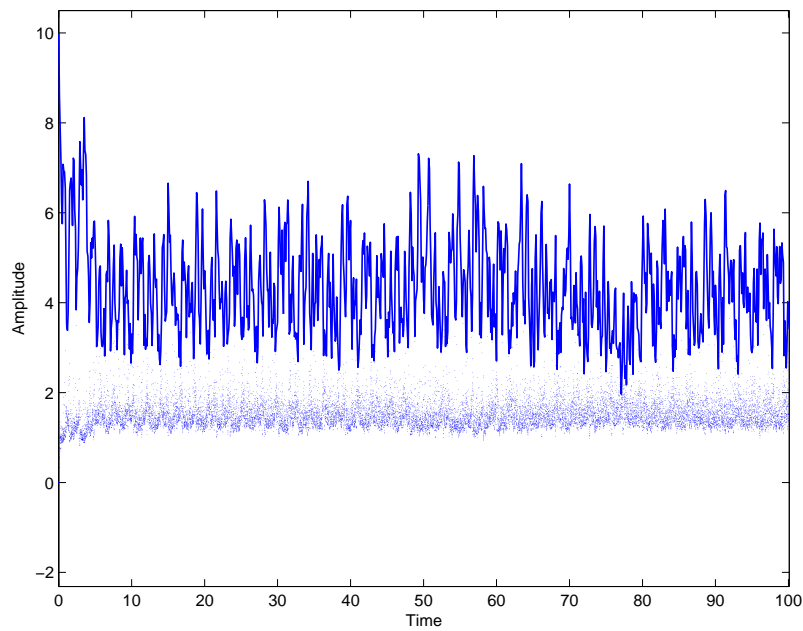


Fig. 84. Solitary wave with tail and wave packet. Amplitudes of the wave-profile maxima against time in case of $\alpha_1 = 0.05$, $\alpha_2 = 0.07$, $\beta = 0.0111$, $n = 1024$, $t_f = 100$, $A = 10$.

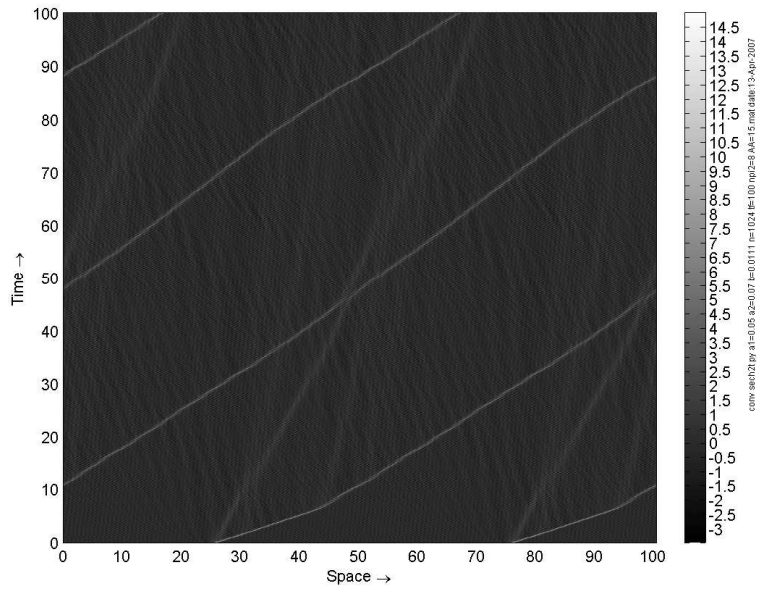


Fig. 85. Solitary wave with tail and wave packet. Pseudocolor plot over two space periods for $\alpha_1 = 0.05$, $\alpha_2 = 0.07$, $\beta = 0.0111$, $n = 1024$, $t_f = 100$, $A = 15$.

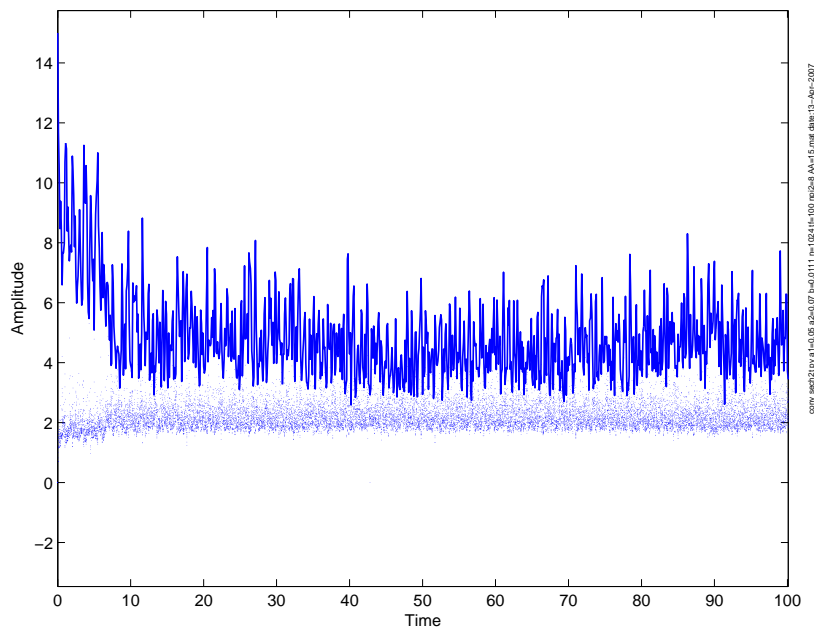


Fig. 86. Solitary wave with tail and wave packet. Amplitudes of the wave-profile maxima against time in case of $\alpha_1 = 0.05$, $\alpha_2 = 0.07$, $\beta = 0.0111$, $n = 1024$, $t_f = 100$, $A = 15$.

The Table 1 summaries the increase of the propagation speed of the (highest) solitary wave in case of increased value of initial amplitude. In all cases the speed of the (highest) solitary wave increases if initial amplitude increases.

Table 1

The speed of the highest (KdV) soliton against the initial amplitude A and solution types.

Type	$A = 1$	$A = 5$	$A = 10$	α_1	α_2	β
1	0.33	1.65	3.26	0.05	0.05	1.111
2	0.58	2.65	5.13	1	0.1	111.11
3	0.41	2.01	3.99	0.1	0.05	111.11
4	0.23	1.03	2.04	0.03	0.09	11.111
5	0.31	1.17	2.17	0.1	0.05	0.1111

9 Wave packet phenomenon and spectral quantities

In the present section the fifth solution type and wave packet phenomenon are discussed in terms of spectral quantities. For this reason spectral densities and time averaged normalised spectral densities are defined. The idea of applying time averaged normalised spectral densities comes from [20] where "time average energies of single modes" are used in order to discuss the energy equipartition in systems of FPU type.

If $U(k, t)$ is the DFT of function $u(x, t)$, defined by expression (3), then spectral densities

$$\begin{aligned} S(k, t) &= \frac{4(U(k, t))^2}{n^2}, & k = 1, \dots, \frac{n}{2} - 1, \\ S(k, t) &= \frac{2(U(k, t))^2}{n^2}, & k = \frac{n}{2}. \end{aligned} \quad (14)$$

For each value of t one can define the sum of spectral densities

$$S_{sum}(t) = \sum_{k=1}^{n/2} S(k, t), \quad (15)$$

normalised spectral densities

$$S_{norm}(k, t) = \frac{S(k, t)}{S_{sum}(t)} \cdot 100\% \quad (16)$$

and time averaged normalised spectral densities (TANSD)

$$S_a(k, t) = \frac{\int_0^t S_{norm}(k, t) dt}{t}. \quad (17)$$

We have discrete values of spectral densities S and S_{norm} at discrete time moments t_i , i.e. we have $S(k, t_i)$ and $S_{norm}(k, t_i)$. Therefore at $t = t_i$

$$S_a(k, t_i) = \frac{\sum_{m=1}^i S_{norm}(k, t_m)}{i}. \quad (18)$$

TANSD (18) reflect the contribution of the k -th spectral density (or amplitude) over the time interval $[0, t_i]$. Compared with spectral densities (or amplitudes) TANSD curves give more clear understanding about domination of certain harmonics.

In case of first four solution types there does not exist dominating spectral densities. For example, in Fig. 87 time averaged spectral densities are plotted

for the third solution type (KdV soliton ensemble with weak tail, see corresponding time–slice plot in Fig. 7). One can see that at $t = 100$ all time averaged spectral densities have values below 2.

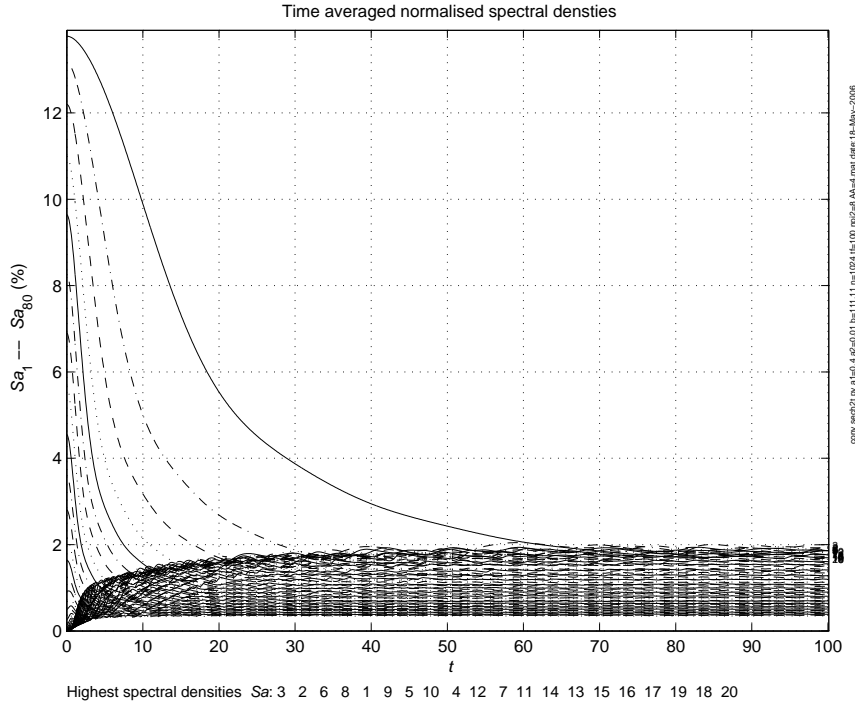


Fig. 87. KdV soliton ensemble with weak tail. Time averaged normalised spectral densities in case of $\alpha_1 = 0.4$, $\alpha_2 = 0.01$, $\beta = 111.11$, $n = 1024$, $t_f = 100$, $A = 4$.

In case of the fifth solution type — solitary wave with tail and wave packet — the behaviour of TANSND is completely different. In Fig. 88 corresponding time-slice plot is presented for $\alpha_1 = 0.05$, $\alpha_2 = 0.09$, $\beta = 0.0111$. TANSND in Fig. 89 demonstrate that $S_a(60, 100) > 40$, $S_a(61, 100) \approx 12.5$, $S_a(59, 100) \approx 11$, $S_a(62, 100) \approx 2.5$ and other TANSND have values less than 2 at $t = 100$, i.e., 59th–62nd spectral densities are amplified and dominate over the others in time interval $[0, 100]$. In Fig. 90 spectral densities are plotted against time for the same case. It is clear that TANSND S_a (compared with spectral densities S) give more clear picture on the contribution of different harmonics.

Two other examples are presented in Figs. 91–94. For $\alpha_1 = 0.01$, $\alpha_2 = 0.005$, $\beta = 0.0111$ (Figs. 91 and 92) there are two groups of amplified harmonics — 82nd and 83rd form the first one and 90th–92nd the second. For $\alpha_1 = 0.05$, $\alpha_2 = 0.11$, $\beta = 0.0111$ (Figs. 93 and 94) 54th–58th harmonics are amplified and dominate over the others. Throughout our numerical experiments only relatively high number harmonics were amplified.

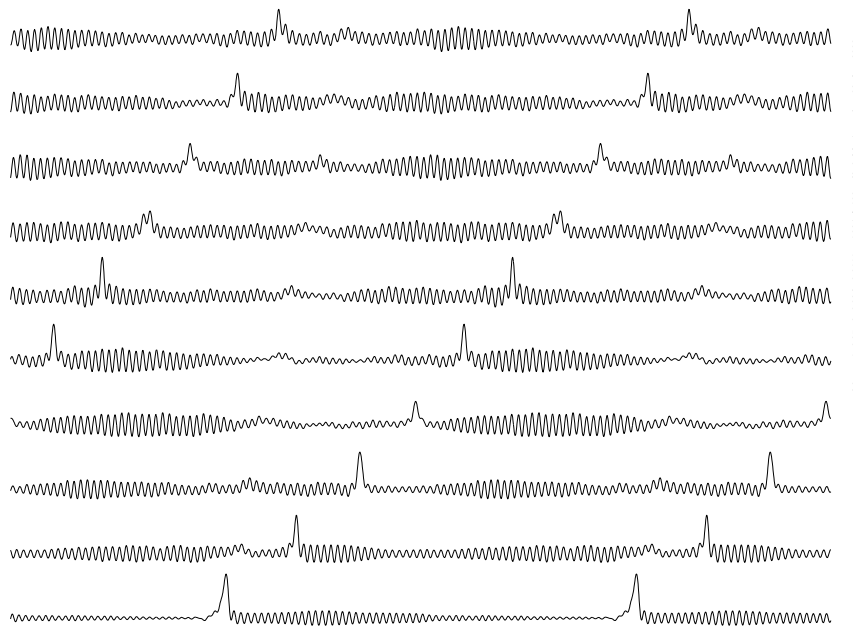


Fig. 88. Solitary wave with tail and wave packet. Time-slice plot over two space periods for $\alpha_1 = 0.05$, $\alpha_2 = 0.09$, $\beta = 0.0111$, $n = 1024$, $t_f = 100$, $A = 4$.

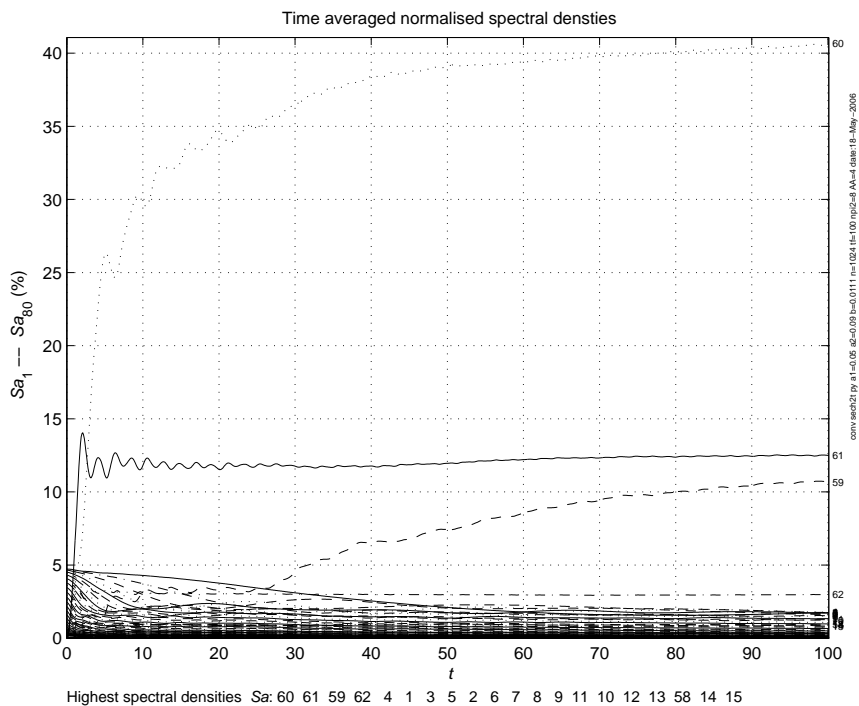


Fig. 89. Solitary wave with tail and wave packet. Time averaged normalised spectral densities in case of $\alpha_1 = 0.05$, $\alpha_2 = 0.09$, $\beta = 0.0111$, $n = 1024$, $t_f = 100$, $A = 4$.

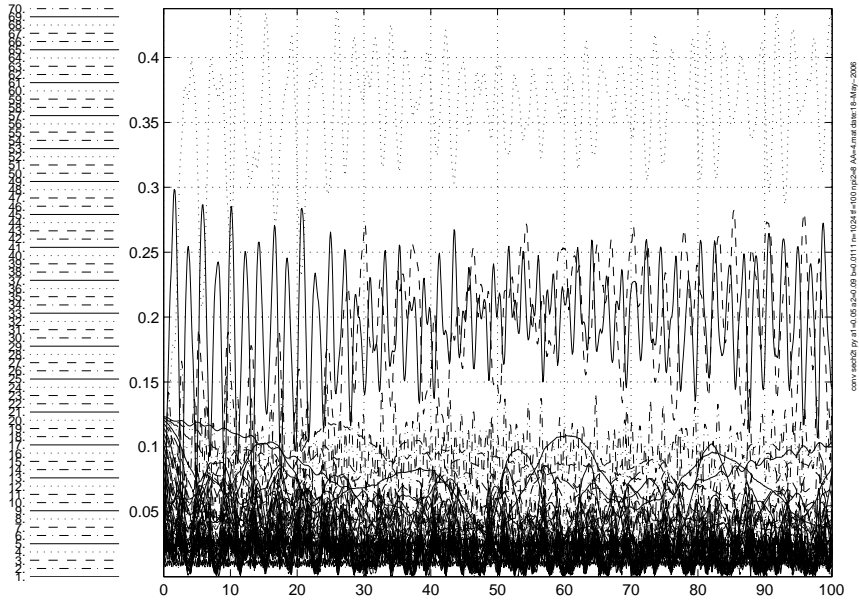


Fig. 90. Solitary wave with tail and wave packet. The 59,60,61, 62 harmonics are amplified. Spectral densities in case of $\alpha_1 = 0.05$, $\alpha_2 = 0.09$, $\beta = 0.0111$, $n = 1024$, $t_f = 100$, $A = 4$.

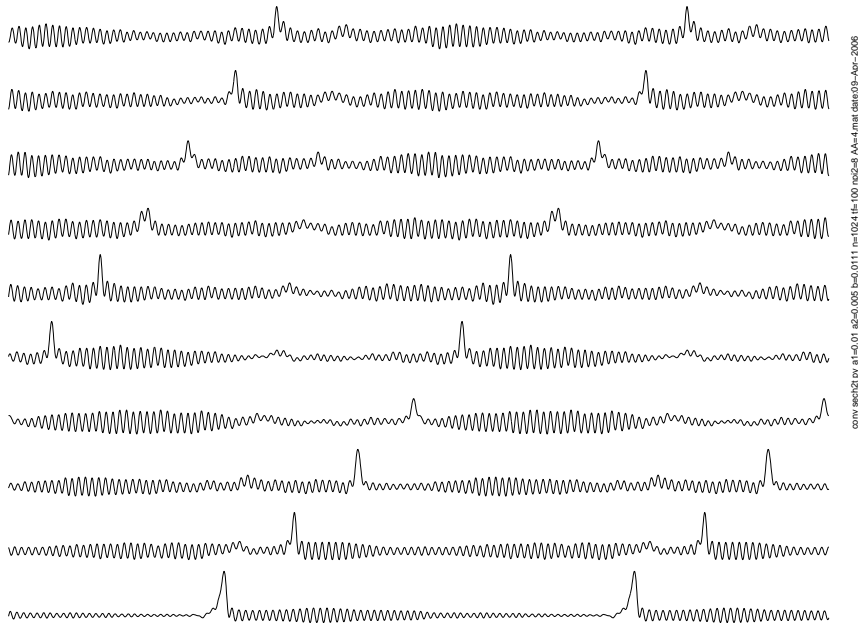


Fig. 91. Solitary wave with tail and wave packet. Time-slice plot over two space periods for $\alpha_1 = 0.01$, $\alpha_2 = 0.005$, $\beta = 0.0111$, $n = 1024$, $t_f = 100$, $A = 4$

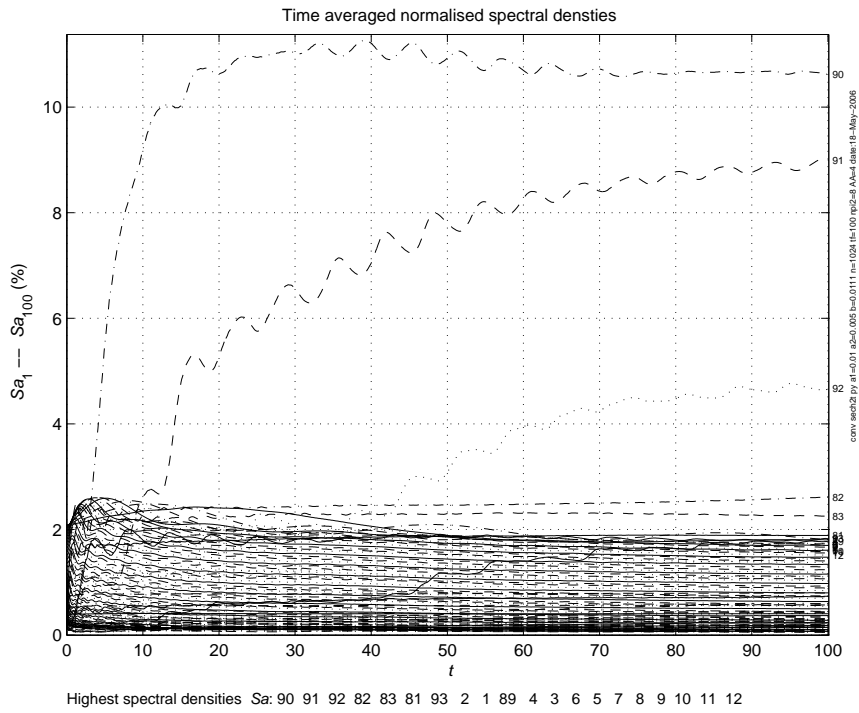


Fig. 92. Solitary wave with tail and wave packet. Time averaged normalised spectral densities in case of $\alpha_1 = 0.01$, $\alpha_2 = 0.005$, $\beta = 0.0111$, $n = 1024$, $t_f = 100$, $A = 4$.

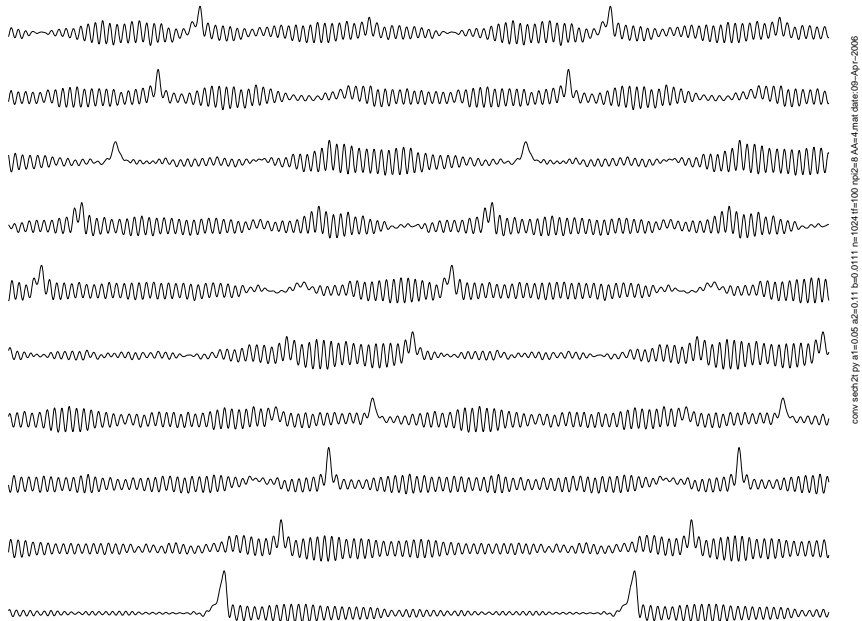


Fig. 93. Solitary wave with tail and wave packet. Time-slice plot over two space periods for $\alpha_1 = 0.05$, $\alpha_2 = 0.11$, $\beta = 0.0111$, $n = 1024$, $t_f = 100$, $A = 4$.

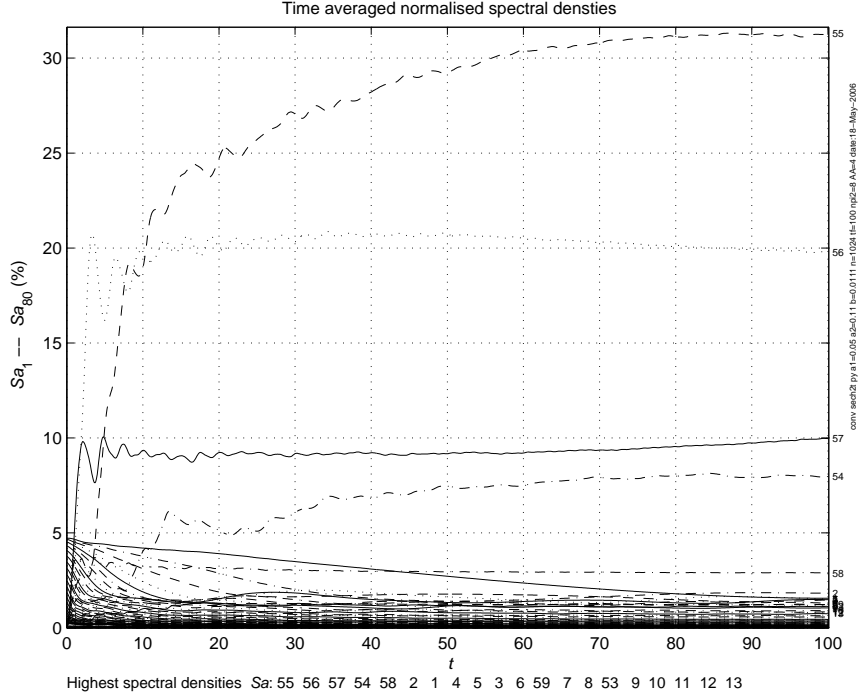


Fig. 94. Solitary wave with tail and wave packet. Time averaged normalised spectral densities in case of $\alpha_1 = 0.05$, $\alpha_2 = 0.11$, $\beta = 0.0111$, $n = 1024$, $t_f = 100$, $A = 4$.

It is clear that wave packets are formed by amplified harmonics and the S_a having the highest value determines the number of maxima (oscillations) in a certain wave profile. Similar situations are described in many textbooks (see [21] for example) in order to explain group velocity and dispersion phenomena — sum of harmonic waves having nearly equal frequencies presents a wave packet.

In the limit case only one spectral density is amplified and "envelope waves" (typical for wave packets) form only in the beginning of integration interval. For $t = t_f$ ensemble of (nearly) equal amplitude of (small) solitary waves (EA ensemble for short) is formed between KdV solitons. EA ensemble was found to form in few cases only and two examples are presented here. For $\alpha_1 = 0.05$, $\alpha_2 = 0.07$, $\beta = 0.0111$ (Figs. 95–97) the 67th harmonic and for $\alpha_1 = 0.07$, $\alpha_2 = 0.11$, $\beta = 0.0111$ (Figs. 98–100) the 63rd harmonic dominates. The number of the dominating harmonic reflects the number of solitary waves in the EA ensemble, i.e. if the 67th is dominating then there is 67 solitary waves in the EA ensemble. Typical EA ensembles can be found in Figs. 95 and 98 at $t = t_f$. Figs. 96, 97, 99 and 100 demonstrate again that time averaged spectral densities S_a (compared with spectral densities S) give more clear picture on the contribution of different harmonics.

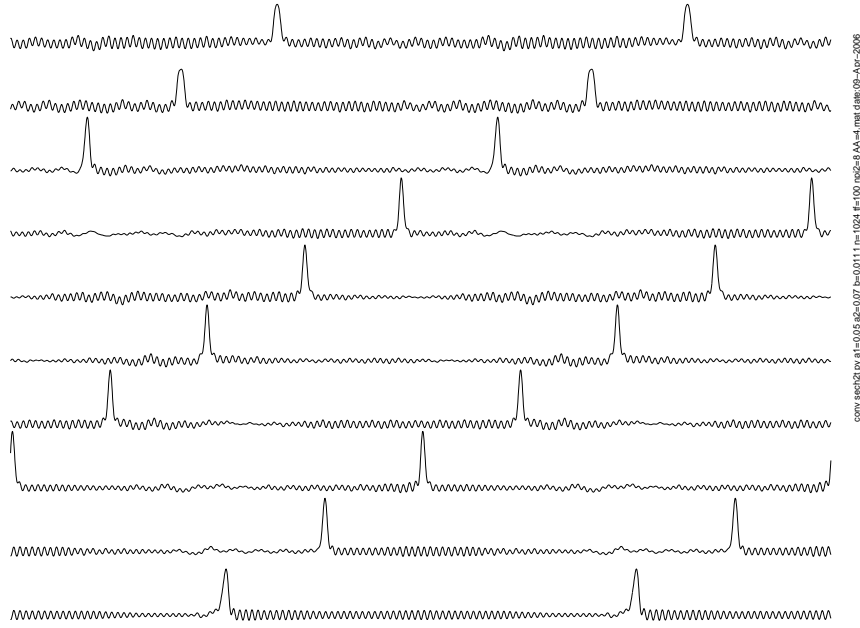


Fig. 95. Solitary wave with tail and wave packet, limite case: KdV soliton with tail and EA ensemble. Time-slice plot over two space periods for $\alpha_1 = 0.05$, $\alpha_2 = 0.07$, $\beta = 0.0111$, $n = 1024$, $t_f = 100$, $A = 4$.

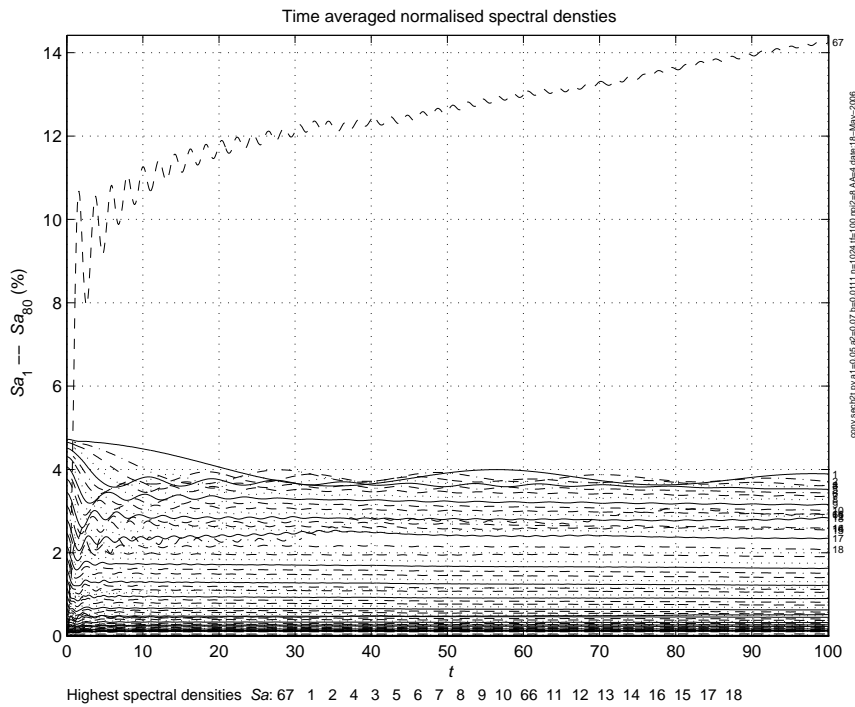


Fig. 96. Solitary wave with tail and wave packet, limite case: KdV soliton with tail and EA ensemble. Time averaged normalised spectral densities in case of $\alpha_1 = 0.05$, $\alpha_2 = 0.07$, $\beta = 0.0111$, $n = 1024$, $t_f = 100$, $A = 4$.

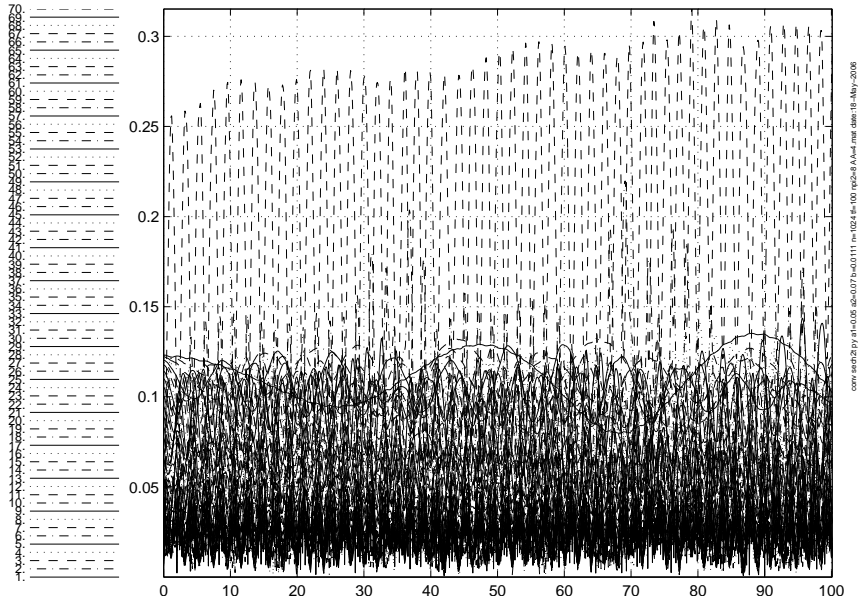


Fig. 97. Solitary wave with tail and wave packet, limite case: KdV soliton with tail and EA ensemble. The 67th harmonic is amplified. Spectral densities in case of $\alpha_1 = 0.05$, $\alpha_2 = 0.07$, $\beta = 0.0111$, $n = 1024$, $t_f = 100$, $A = 4$.

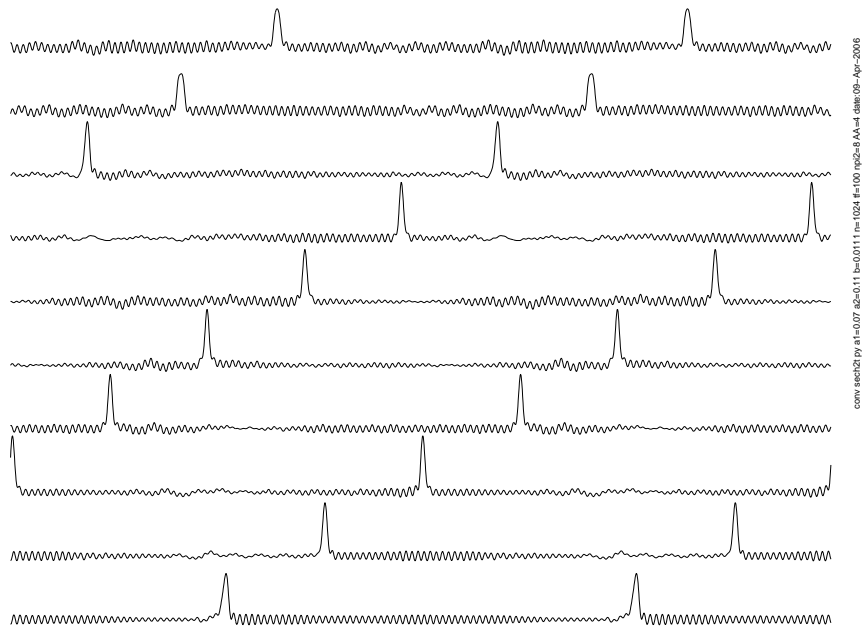


Fig. 98. Solitary wave with tail and wave packet, limite case: KdV soliton with tail and EA ensemble. Time-slice plot over two space periods for $\alpha_1 = 0.07$, $\alpha_2 = 0.11$, $\beta = 0.0111$, $n = 1024$, $t_f = 100$, $A = 4$.

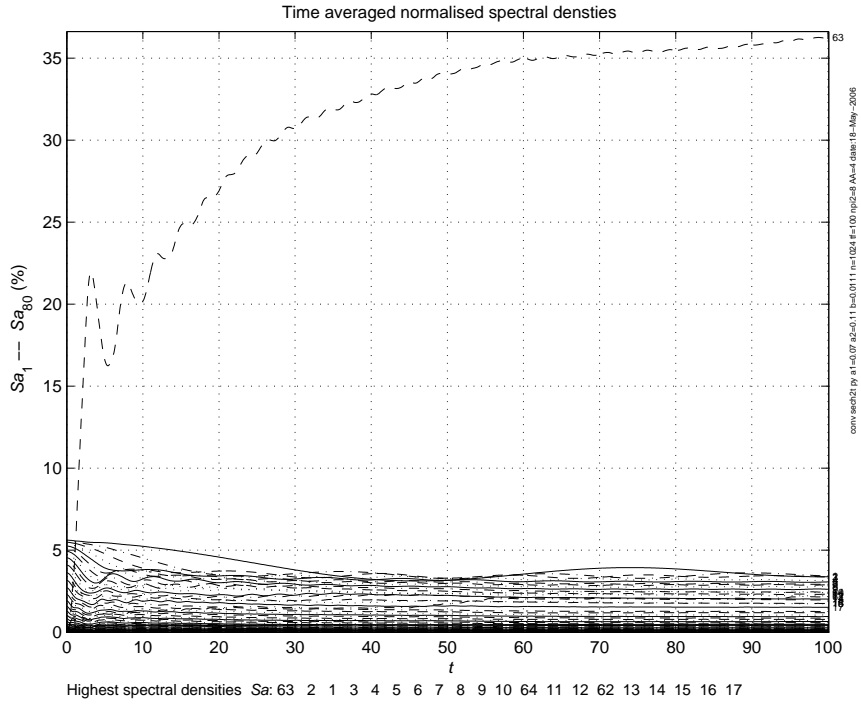


Fig. 99. Solitary wave with tail and wave packet, limite case: KdV soliton with tail and EA ensemble. Time averaged normalised spectral densities in case of $\alpha_1 = 0.07$, $\alpha_2 = 0.11$, $\beta = 0.0111$, $n = 1024$, $t_f = 100$, $A = 4$.

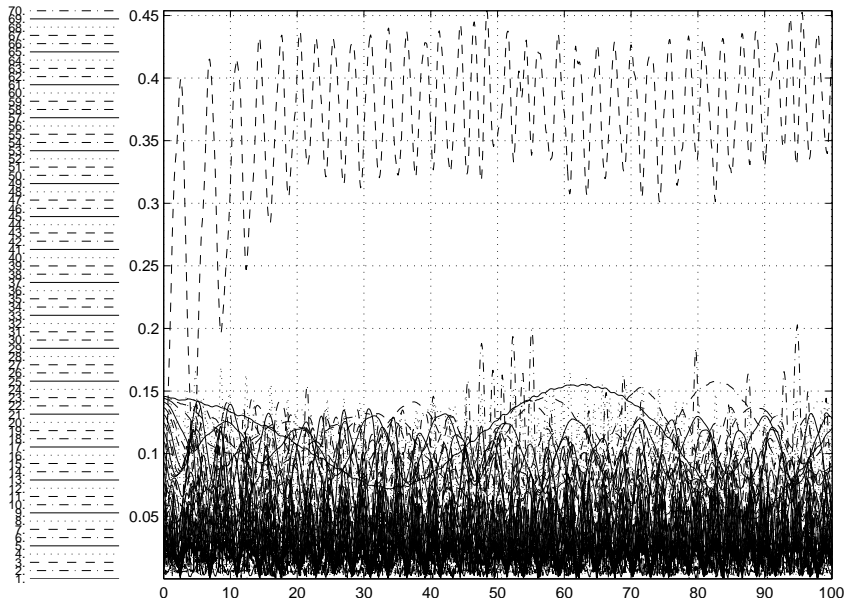


Fig. 100. Solitary wave with tail and wave packet, limite case: KdV soliton with tail and EA ensemble. The 63rd harmonic is amplified. Spectral densities in case of $\alpha_1 = 0.07$, $\alpha_2 = 0.11$, $\beta = 0.0111$, $n = 1024$, $t_f = 100$, $A = 4$.

10 Conclusions

In the present paper propagation of solitary waves in dilatant granular materials is studied. HKdV Eq. (1) is integrated numerically under sech^2 type localised initial conditions and time-space behaviour of solutions is analysed over wide range of dispersion parameters α_1 , α_2 , and microstructure parameter β .

The main results of the current study are:

- (1) Depending on the character of solutions five solution types are defined:
 - Single KdV soliton;
 - KdV soliton ensemble;
 - KdV soliton ensemble with weak tail;
 - Soliton with strong tail;
 - Solitary wave with tail and wave packet.
- (2) The solitonic character of the solution is discussed for all solution types.
 - First solution type — soliton — the initial solitary wave which is the analytical solution of the KdV equation propagates at constant speed and amplitude.
 - Second solution type — soliton — KdV solitons conserve their shape and speed throughout interactions with other KdV solitons.
 - Third solution type — soliton — solitary waves restore their speed and shape after interactions, i.e., their behaviour is very close to that of the KdV solitons and therefore the train of solitary waves is called KdV soliton ensemble.
 - Fourth solution type — soliton like behaviour — the single soliton (almost) conserves its shape and speed throughout interactions with the strong tail.
 - Fifth solution type — soliton like behaviour — the solitary wave conserves its shape and speed throughout interactions with the wave packet and the tail.
- (3) In case of the fourth and the fifth solution type the name KdV soliton for the solitary wave is quite conditional because no interactions between solitary waves take place. However, the single solitary wave interacts with the tail and wave packets and conserves its speed and shape through such interactions.
- (4) The essence of the fifth solution type is analysed in terms of time averaged spectral densities. It has been shown that wave packets are generated by several amplified higher order harmonics that dominate over the lower order harmonics. In the limit case only one amplified harmonic exist and an EA ensemble emerges instead of wave packet(s).
- (5) Dependencies between solution types and material parameters are established (see Figs. 29–33). It has been shown that dispersion parameters

have strong influence on character of the solution — small changes in values of parameters may cause the change of the solution type.

- (6) Behaviour of amplitudes of (KdV) solitons against solution types is analysed (see Figs. 29–33 and 44–48).
- (7) Dependencies between the number of KdV solitons against material parameters is established (see Figs. 49–53).
- (8) The influence of the amplitude of the initial solitary wave on the character of the solution is analysed. It has been shown that the higher the amplitude of the initial solitary wave the higher the speed of the KdV solitons. However, the essence of the solution type remains the same.

The most interesting phenomenon here is related to the fifth solution type, i.e., to the simultaneous emergence of the solitary wave, the tail and the wave packet. The long-time behaviour of this phenomenon needs further examination. Corresponding numerical simulations and detail analysis is in the progress.

Acknowledgements

Authors of this paper thank Professor Jüri Engelbrecht for helpful discussions and Dr. Pearu Peterson for Python related scientific software developments and assistance. The research was partially supported by Estonian Science Foundation Grant No 7035 (A.S. and L.I.) and EU Marie Curie Transfer of Knowledge project MTKD-CT-2004-013909 under FP 6 (A.S.).

References

- [1] P. Giovine, F. Oliveri, Dynamics and wave propagation in dilatant granular materials, *Meccanica* 30 (1995) 341–357.
- [2] F. Oliveri, Wave propagation in granular materials as continua with microstructure: Application to seismic waves in a sediment filled site, *Rendiconti Circolo Matematico di Palermo* 45 (1996) 487–499.
- [3] G. Cataldo, F. Oliveri, Nonlinear seismic waves: A model for site effects, *Int. J. Non-linear Mech.* 34 (1999) 457–468.
- [4] G. Whitham, *Linear and Nonlinear Waves*, John Wiley & Sons, 1974.
- [5] M. Remoissenet, *Waves Called Solitons: Concepts and Experiments*, Springer-Verlag, Berlin et al., 1994.
- [6] P. G. Drazin, *Solitons*, Cambridge University Press, Cambridge et al., 1983.

- [7] P. G. Drazin, R. S. Johnson, *Solitons: an Introduction*, Cambridge University Press, Cambridge et al., 1989.
- [8] N. Zabusky, Computational synergetics and mathematical innovation, *J. Comp. Phys.* 43 (1981) 195–249.
- [9] N. J. Zabusky, M. D. Kruskal, Interaction of solitons in a collisionless plasma and the recurrence of initial states, *Phys. Rev. Lett.* 15 (1965) 240–243.
- [10] H.-O. Kreiss, J. Olinger, Comparison of accurate methods for the integration of hyperbolic equations, *Tellus* 30 (1972) 341–357.
- [11] A. Salupere, On the application of the pseudospectral method for solving the Korteweg–de Vries equation, *Proc. Estonian Acad. Sci. Phys. Math.* 44 (1) (1995) 73–87.
- [12] A. Salupere, On the application of pseudospectral methods for solving nonlinear evolution equations, and discrete spectral analysis, in: *Proc. of 10th Nordic Seminar on Computational Mechanics*, Tallinn, TTU, 1997, pp. 76–83.
- [13] B. Fornberg, *Practical guide to pseudospectral methods*, Cambridge University Press .
- [14] E. Jones, T. Oliphant, P. Peterson, et al., *SciPy: Open source scientific tools for Python*, <http://www.scipy.org> (2007).
- [15] M. Frigo, S. G. Johnson, The design and implementation of FFTW3, *Proceedings of the IEEE* 93 (2) (2005) 216–231.
- [16] P. Peterson, F2PY: Fortran to Python interface generator, <http://cens.ioc.ee/projects/f2py2e/> (2005).
- [17] A. C. Hindmarsh, Odepack, a systematized collection of ODE solvers, in: R. S. Stepleman, et al. (Eds.), *Scientific Computing*, North-Holland, Amsterdam, 1983, pp. 55–64.
- [18] A. V. Porubov, *Amplification of Nonlinear Strain Waves in Solids*, World Scientific, Singapore, 2003.
- [19] C. Christov, M. Velarde, Dissipative solitons, *Physica D* 86 (1995) 323–347.
- [20] L. Galgani, A. Giorgilli, A. Martinoli, S. Vanzini, On the problem of energy equipartition for large systems of the Fermi–Pasta–Ulam type: analytical and numerical estimates, *Physica D* 59 (1992) 334–348.
- [21] J. Billingham, A. King, *Wave Motion*, Cambridge University Press, Cambridge et al., 2000.